Experimental Cerebral Malaria Pathogenesis—Hemodynamics at the Blood Brain Barrier

Adéla Nacer[1¤a], Alexandru Movila[1¤b], Fabien Sohet[2¤c], Natasha M. Girgis[1], Uma Mahesh Gundra[1], P'ng Loke[1], Richard Daneman[2¤c], Ute Frevert[1]*

1 Department of Microbiology, Division of Medical Parasitology, New York University School of Medicine, New York, New York, United States of America, 2 Department of Anatomy, University of California San Francisco, San Francisco, California, United States of America

Abstract

Cerebral malaria claims the lives of over 600,000 African children every year. To better understand the pathogenesis of this devastating disease, we compared the cellular dynamics in the cortical microvasculature between two infection models, *Plasmodium berghei* ANKA (PbA) infected CBA/CaJ mice, which develop experimental cerebral malaria (ECM), and *P. yoelii* 17XL (PyXL) infected mice, which succumb to malarial hyperparasitemia without neurological impairment. Using a combination of intravital imaging and flow cytometry, we show that significantly more CD8+ T cells, neutrophils, and macrophages are recruited to postcapillary venules during ECM compared to hyperparasitemia. ECM correlated with ICAM-1 upregulation on macrophages, while vascular endothelia upregulated ICAM-1 during ECM and hyperparasitemia. The arrest of large numbers of leukocytes in postcapillary and larger venules caused microrheological alterations that significantly restricted the venous blood flow. Treatment with FTY720, which inhibits vascular leakage, neurological signs, and death from ECM, prevented the recruitment of a subpopulation of CD45^{hi} CD8+ T cells, ICAM-1+ macrophages, and neutrophils to postcapillary venules. FTY720 had no effect on the ECM-associated expression of the pattern recognition receptor CD14 in postcapillary venules suggesting that endothelial activation is insufficient to cause vascular pathology. Expression of the endothelial tight junction proteins claudin-5, occludin, and ZO-1 in the cerebral cortex and cerebellum of PbA-infected mice with ECM was unaltered compared to FTY720-treated PbA-infected mice or PyXL-infected mice with hyperparasitemia. Thus, blood brain barrier opening does not involve endothelial injury and is likely reversible, consistent with the rapid recovery of many patients with CM. We conclude that the ECM-associated recruitment of large numbers of activated leukocytes, in particular CD8+ T cells and ICAM+ macrophages, causes a severe restriction in the venous blood efflux from the brain, which exacerbates the vasogenic edema and increases the intracranial pressure. Thus, death from ECM could potentially occur as a consequence of intracranial hypertension.

Data Availability: The authors confirm that all data underlying the findings are fully available without restriction. All relevant data are within the paper and its Supporting Information files.

Competing Interests: The authors have declared that no competing interests exist.

* Email: ute.frevert@nyumc.org

¤a Current address: Bacteriology Division, NIBSC-MHRA, South Mimms, Potters Bar, Hertfordshire, United Kingdom
¤b Current address: Department of Immunology and Infectious Diseases, The Forsyth Institute, Cambridge, Massachusetts, United States of America
¤c Current address: Department of Pharmacology, University of California San Diego, La Jolla, California, United States of America

Introduction

Plasmodium falciparum is responsible for an estimated 600,000 deaths annually, principally in children under the age of five [1]. Clinical symptoms range from intermittent fevers and chills to potentially fatal complications including severe anemia and cerebral malaria [2]. The mortality rate in comatose pediatric patients, most frequently due to respiratory arrest, is 15–20% despite optimal medical care [3], but the underlying pathology is unclear.

Molecular and cellular mechanisms involved in the pathogenesis of human cerebral malaria (HCM) include a predominantly pro-inflammatory cytokine profile, endothelial activation via the NF-κB pathway with upregulation of adhesion molecules, glia cell activation, and sequestration of infected red blood cells (iRBC),

monocytes, and platelets within brain capillaries [3–6]. However, the cellular mechanisms associated with HCM cannot be directly observed in the human brain. Ophthalmological examination of the retinal pathology generally correlates with course and etiology of malarial encephalopathy [2,7], but despite significant recent improvements [8], this technique lacks the resolution to observe the dynamic behavior of individual iRBC, leukocytes, and platelets, their exact location within the microvasculature, mechanisms of vascular leakage or possibly occlusion, and the sequence of these events. Elucidation of CM pathogenesis therefore requires the use of a robust small animal model that closely reflects clinical symptoms, histopathology, and immune mechanisms associated with the pathophysiology of HCM.

P. berghei ANKA (PbA) infected CBA, Swiss Webster, or CB57Bl/6 mice represent a well-characterized and widely used

Author Summary

Malaria remains one of the most serious health problems globally, but our understanding of the biology of the *Plasmodium* parasite and the pathogenesis of severe disease is still limited. Human cerebral malaria (HCM), a severe neurological complication characterized by rapid progression from headache to convulsions and unrousable coma, causes the death of hundreds of thousands of children in Africa annually. To better understand the pathogenesis of cerebral malaria, we imaged immune cells in brain microvessels of mice with experimental cerebral malaria (ECM) versus mice with malarial hyperparasitemia, which lack neurological impairment. Death from ECM closely correlated with plasma leakage, platelet marginalization, and the recruitment of significantly more leukocytes to postcapillary venules compared to hyperparasitemia. Leukocyte arrest in postcapillary venules caused a severe restriction in the venous blood flow and the immunomodulatory drug FTY720 prevents this recruitment and death from ECM. We propose a model for ECM in which leukocyte arrest, analogous to the sequestration of *P. falciparum* infected red blood cells in HCM, severely restricts the venous blood flow, which exacerbates edema and swelling of the brain at the agonal comatose stage of the infection, leading to intracranial hypertension and death.

model for experimental cerebral malaria (ECM) that shares a number of similarities with *P. falciparum* HCM [5,6,9–12]. Both ECM and HCM are characterized by severe vasculopathy, i.e. endothelial activation and dysfunction with increased expression of adhesion molecules such as ICAM-1, VCAM-1, and E-selectin, upregulation of inflammatory cytokines, reduced blood flow, vascular leakage, acute edema of both vasogenic and cytotoxic origin, and microhemorrhages leading to neurological impairment [12–17]. Platelet activation, dysregulation of the coagulation cascade, thrombocytopenia, and platelet accumulation in the brain are also found in both HCM and ECM [18–20]. We have previously shown by intravital microscopy (IVM) that platelet marginalization and blood brain barrier (BBB) disruption are central to ECM pathophysiology [21]. Platelets are thought to impair vascular repair and increase BBB permeability by potentiating the iRBC-induced endothelial damage in the early stages of HCM development [22–24]. Circulating platelet-derived microparticles are increased in severe *P. falciparum* malaria and serve as a biomarker for neurological involvement [13,25].

The murine PbA model has also provided ample evidence for a contribution of CD8+ and CD4+ T cells to the late stages of ECM development [26–30]. Both CD8+ T cells, generally considered the terminal effector cells, and CD4+ T cells must accumulate in the cerebral microvasculature for ECM to occur [11,27,28,31–35] and may also be responsible for the ECM-associated leukocyte infiltration [36]. While ECM development was thought to involve CD8+ T cell-induced endothelial apoptosis via perforin- and granzyme B-mediated cytotoxicity resulting in BBB disruption [32,33,37], we recently showed by IVM that ECM closely correlates with widespread opening of the BBB and that this occurs in the absence of significant endothelial death [21]. The BBB at the level of postcapillary venules encompasses two layers, the vascular endothelium with its basement membrane and the glia limitans with associated basement membranes and astrocyte endfeet, which are separated by the perivascular space [38]. This section of the BBB is functionally distinct from other areas of the

BBB, for example that at the capillary level, which consists of a single layer composed of endothelia, gliovascular membrane, and astrocyte endfeet [38]. IVM also revealed that ECM correlates with platelet deposition, leukocyte arrest, and *de novo* expression of the pattern recognition receptor CD14 on the endothelial surface from postcapillary venules, but not from capillaries or arterioles [21]. Strikingly, inhibition of platelet deposition and leukocyte recruitment by blockage of LFA-1 mediated cellular interactions prevented ECM and disruption of the BBB in PbA-infected mice [21]. Thus, it appears that the ultimate cause of coma and death in ECM is a universal breakdown of the BBB at the level of postcapillary venules [21].

In the PbA-infected CBA/CaJ mouse model, vascular leakage, neurological signs, and death from ECM can be prevented by treatment with the endothelial barrier-stabilizing sphingosine 1 analog FTY720 (fingolimod) [21,39], an immunomodulatory FDA-approved drug for oral treatment of relapsing multiple sclerosis (MS) [40] that acts as an agonist for sphingosine 1-phosphate (S1P) receptors [41]. In experimental autoimmune encephalomyelitis (EAE), FTY720 prevents T cell recruitment to the brain by down-modulating the expression of S1P1 receptors on the T cell surface. This favors the CCR7-mediated retention of naïve and central memory T cells within secondary lymphatic tissues [42], leading to a reduction in the numbers of naïve and central memory T cells, but not effector memory T cells, in the blood [43]. FTY720 may also prevent stimulation of vascular endothelia or activation of CD8+ effector T cells in the spleen by decreasing CD11c+ DC migration and function and by destabilizing DC/T cell interactions thus preventing the formation of an immunological synapse [44,45]. In addition to its involvement in T cell activation and targeting to the brain, FTY720 is also thought to have a directly stabilizing effect on endothelial junctions at the BBB [46–49]. However, the exact mechanism by which FTY720 prevents BBB opening remains unclear to date.

Here, we show that ECM is associated with the accumulation of numerous leukocytes within postcapillary and larger venules and that the resulting microrheological alterations severely restrict the venous blood flow. Treatment with FTY720 significantly reduced the recruitment of these leukocytes indicating their involvement in the pathogenesis of ECM [21,39]. Leukocyte arrest likely increases the intracranial pressure, similarly to *P. falciparum* iRBC sequestration in pediatric HCM, which is typically associated with a poor clinical outcome [50].

Results

Three week-old CBA/CaJ mice were infected with PbA-GFP or *P. yoelii* 17XL (PyXL)-RFP and monitored throughout the course of development of ECM or hyperparasitemia [21]. In this study, a total of 78 PbA-infected mice were subjected to IVM at the time of ECM (day 6–8), 18 PbA-infected mouse before ECM (day 5), 15 PbA-infected mice that failed to develop ECM (day 9), and 25 uninfected control mice (**Table S1**). We also examined 30 PbA-infected mice that were treated with FTY720 and failed to develop ECM (day 8–9) and 8 PbA-infected mice that developed ECM on day 8 despite treatment with FTY720. As controls for parasitemia, 62 PyXL-infected mice with >50% parasitemia (day 5) were analyzed. Throughout our IVM experiments, we examined deep microvessels, i.e. branches of penetrating arterioles and venules [51,52], which were in direct continuation with the cortical capillary bed. Imaging of CX3CR1$^{GFP/+}$ mice confirmed that the postcapillary venules, capillaries, and arterioles used for analysis are embedded in fluorescent microglia and thus clearly located in

the cerebral cortex, i.e. underneath the pial microvasculature (**Figure S1**) [21].

ECM correlates with microrheological alterations in postcapillary venules

IVM revealed that the venous blood flow in postcapillary venules from PbA-infected mice with neurological signs (day 6) was strikingly altered. Vascular labeling with Evans blue revealed that postcapillary venules from mice with ECM exhibited a marginal zone devoid of RBCs (**Figure 1A, Video S1**). Instead, this zone contained variable numbers of leukocytes that were either rolling along the endothelium, crawling, or firmly attached (**Figure S2A and S2C, Video S2**). Minimal projections of time sequences emphasize the boundary between the functional lumen in the center of the postcapillary venules and the RBC-free marginal zone and suggest that the functional lumen available for the blood flow is significantly restricted during ECM (**Figure S2B and S2D**). This phenomenon was even more pronounced in larger venules. Neither arterioles from mice with ECM (**Figure 1B, Video S3**) nor postcapillary venules or arterioles from mice with hyperparasitemia (**Figure 1C and 1D, Video S4**) showed any significant functional vascular restriction, i.e. narrowing of the passageway available for the blood flow, compared to uninfected control mice (**Figure 1E and 1F, Video S5**), a finding we attribute to the absence of steric hindrance generated by adherent leukocytes in these vessels. Multiple measurements of the total vascular diameter (from endothelium to endothelium) and the functional diameter (used by the blood flow) of 50 randomly chosen postcapillary venules from 4 mice with ECM revealed a mean functional diameter of $70.5 \pm 13.7\%$ compared to data from 3 uninfected control mice, corresponding to a functional vascular cross-section of $55.8 \pm 19.1\%$ (**Figure 1G**). Notably, complete vascular occlusion, whether in postcapillary venules or other microvessels, was not observed during ECM. In 50 randomly chosen postcapillary venules from 3 PyXL-infected mice with hyperparasitemia, the functional postcapillary venule diameter and cross-section was $95.5 \pm 3.4\%$ and $92.7 \pm 5.1\%$, respectively. No microrheological alterations were found in postcapillary venules or arterioles from PbA-infected mice prior to ECM (day 5), in PbA-infected mice that failed to develop ECM (day 9), or in uninfected control mice. As reported previously [21], PbA-infected mice that did develop ECM despite treatment FTY720 exhibited vascular leakage suggesting that the venous blood flow restriction was similar to untreated PbA-infected mice with ECM.

Thus, ECM correlates with a significant functional constraint, but not complete blockage, of the passageway available for the venous blood flow. This is significant, because any restriction in the venous efflux from the brain likely exacerbates edema formation, a hallmark of both ECM and HCM [16,17,53]. A venous efflux problem would also explain the increased intracranial pressure, which is frequently observed in pediatric CM in Africa [50]. Indeed, MRI imaging has identified increased intracranial pressure as the strongest predictor of death [54,55].

Leukocyte recruitment during ECM and hyperparasitemia

Quantitative offline IVM analysis of the various cell densities revealed that leukocytes are recruited to the cortical microvasculature not only in response to ECM, but also hyperparasitemia, albeit at a significantly lower density (**Figure 2**). Specifically, more CD8+ T cells, neutrophils, and macrophages were recruited in ECM compared to hyperparasitemia, while the density of all other cell types analyzed did not differ between these two infections (**Figure 3A**). The cortical microvasculature of uninfected control mice exhibited virtually no arrested leukocytes suggesting that in

the absence of an inflammatory stimulus, innate immune cells do not monitor the BBB.

CD8+ and CD4+ T cells. On the day of neurological signs, the density of CD8+ T cells arrested in postcapillary venules from PbA-infected mice was 292.1 ± 58.9 cells/mm^2 (**Figure 3A, Table S2**). While 92.7% of these T cells were intravascular, 7.3% had extravasated into the perivascular space. No CD8+ T cells were found on the day prior to ECM or in mice that survived the critical period of ECM development. Interestingly, CD8+ T cells were also found in postcapillary venules from PyXL-infected mice with hyperparasitemia and severe anemia. However, with 61.0 ± 8.1 cells/mm^2, the density was significantly lower (t-test: $T_{(4)} = 8.69$; $P < 0.01$) and no T cells were found in the perivascular space of these mice. CD8+ T cells were absent from the cortical microvasculature of uninfected control mice. Examination of the cellular dynamics by IVM revealed that CD8+ T cells crawled along postcapillary venule endothelia at similar velocities during both ECM and hyperparasitemia (2.98 ± 2.28 μm/min and 3.03 ± 1.62 μm/min, respectively) (**Figure S3, Videos S6 and S7**). No extravascular CD8+ T cells were observed during hyperparasitemia. In agreement with previous reports, no differences were found in CD4+ T cells and densities between PbA and PyXL infections [26] (**Figure 3, Table S3, Video S8 and S9**). Together, these findings suggest that neurological signs and CD8+ T cell recruitment are correlated and occur rapidly.

Neutrophils. Significantly higher numbers of neutrophils were found in PCV and whole brain during ECM compared to HP. The density of GR-1 (Ly6G) positive neutrophils in postcapillary venules from PbA-infected mice with ECM on day 6–8 was 467.6 ± 137.6 cells/mm^2. No neutrophils were detected prior to ECM or in mice that survived the critical period without ECM development (**Figure 3A, Table S4**). PyXL-infected mice also exhibited neutrophils in postcapillary venules, albeit at the significantly lower density of 276.3 ± 65.9 cells/mm^2 at the time of hyperparasitemia (t-test: $T_{(5)} = 2.80$; $P < 0.05$). Uninfected control mice did not exhibit arrested neutrophils. GR-1+ neutrophils did not extravasate into the perivascular space, neither during ECM nor during hyperparasitemia (**Videos S10 and S11**). Further, FTY720 treatment of PbA-infected mice reduced the number of neutrophils significantly so that levels similar to those found during HP were reached (**Figure 3C, Table S7**), which supports the previously suggested involvement of neutrophils in the ECM-associated vasculopathy and edema formation [26].

Monocytes and macrophages. Monocytes were present at similar densities in mice with ECM and HP (**Figure 3, Table S5**), which is consistent with earlier reports showing that monocytes are not involved in iRBC accumulation in the brain at the time of ECM [26]. The density of CD11b+ macrophages, however, was significantly higher during ECM (484.1 ± 13.1 cells/mm^2) compared to during hyperparasitemia (110.2 ± 17.4 cells/mm^2) (t-test: $T_{(2)} = 16.56$; $P < 0.01$; **Figure 3A, Table S6**). In contrast to monocytes, which were exclusively found to be intravascular (**Figure 2, Videos S12 and S13**), CD11b+ macrophages were occasionally observed in the perivascular space (**Figure 2, Videos S14 and S15**). While macrophages could be tissue or blood derived, intravenous labeling suggests that the fluorescent extravascular cells are of the hematopoietic origin. However, we cannot exclude that the cells represent resident perivascular macrophages that were labeled by fluorescent marker leaking into the perivascular space.

Role of S1P receptors. We reported that the immunomodulatory drug FTY720 reduces the overall number of arrested leukocytes in the cortical microvasculature of PbA-infected mice [21,39]. To determine the effect of FTY720 on CD8+ T cell
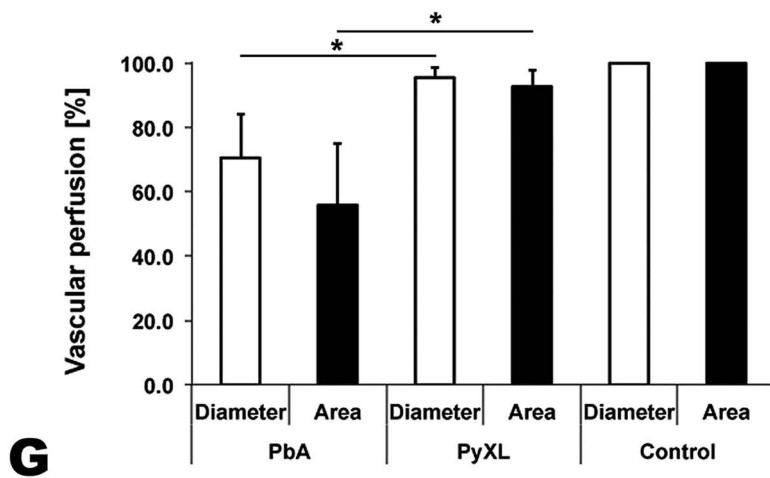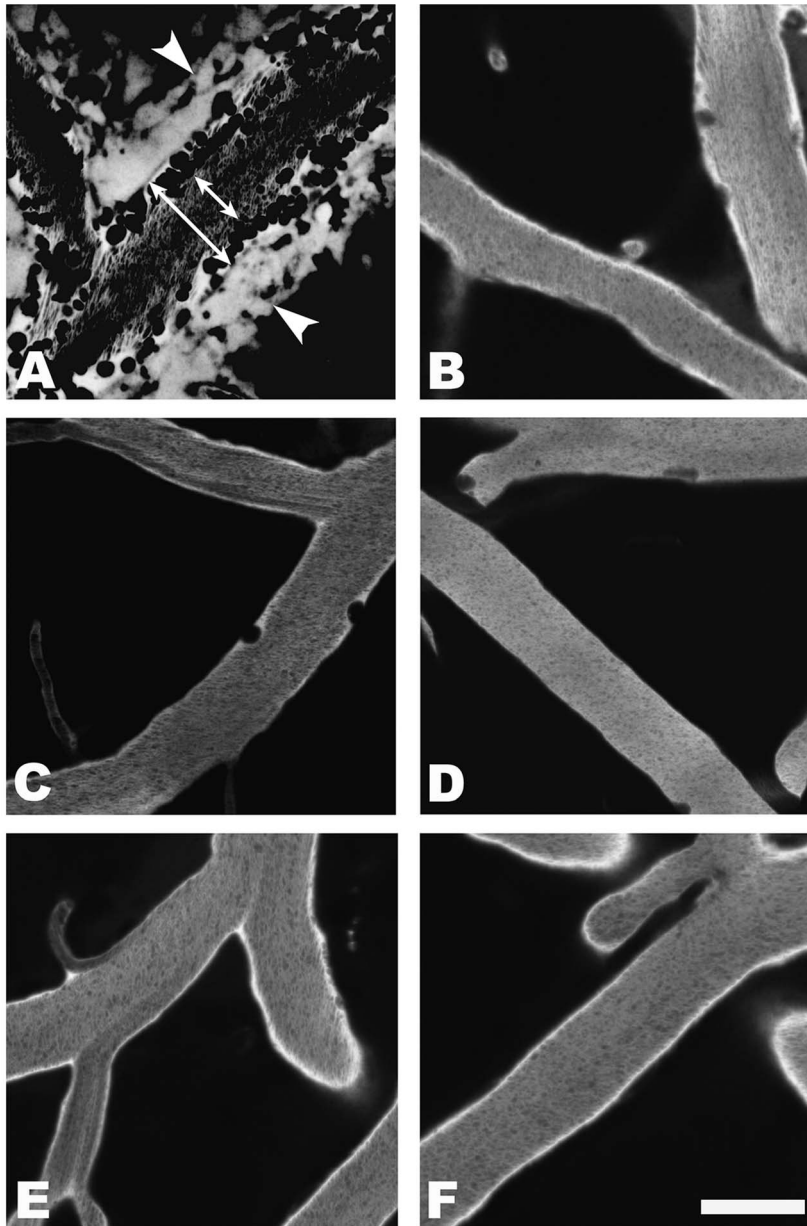
Figure 1. ECM correlates with microrheological alterations in postcapillary venules. CBA/CaJ mice were infected with PbA, PyXL, or no parasites. To assess the blood flow within the cortical microvasculature, time sequences were converted to minimal projections. **A**) In mice with ECM, the functional postcapillary venule diameter (short arrow), i.e. the perfused portion of the vessel, is considerably reduced compared to the entire vessel diameter (long arrow). Visualization of the vascular lumen with Evans blue reveals a zone along the endothelium of postcapillary venules (**A**) that contains adherent leukocytes (dark circles or ovals), but is devoid of RBC (dark streaks in the center). Note that migrating leukocytes are represented multiple times in minimal projections. Leakage of Evans blue into the perivascular space and brain parenchyma is apparent on either side of the postcapillary venule (arrowheads). **B**) Arterioles from mice with symptomatic ECM do not exhibit any restriction in diameter. **C**) The small number of adherent leukocytes (dark circles) in mice with hyperparasitemia does not cause any significant restriction in the functional postcapillary venule lumen. Neither arterioles from mice with hyperparasitemia (**D**) nor postcapillary venules or arterioles from uninfected control mice (**E and F**) exhibit any microrheological alterations. Scale bars = 20 µm. See **Videos S1–S5** for the corresponding dynamic data. **G**) Measurement of the total and functional vascular diameters and cross-sections reveals that the blood flow in postcapillary venules from mice with ECM, but not from mice with hyperparasitemia, is severely restricted. Postcapillary venules from uninfected control mice exhibit no luminal restriction.
doi:10.1371/journal.ppat.1004528.g001

arrest, mice were treated starting on day 1 prior to infection and on days 1, 3, and 5 after infection. FTY720 treatment allowed 73% of the mice to survive the critical period of ECM development (day 6–8) without exhibiting neurological signs until they were analyzed on day 9. Only ECM-negative mice were examined. While postcapillary venules from untreated mice contained 292.1 ± 58.9 CD8+ T cells/mm^2 at the time of neurological signs (**Table S2**), FTY720 treatment significantly reduced the cell density to 81.9 ± 25.9 cells/mm^2 (ANOVA; $F_{(2)} = 59.41$; $P < 0.001$) (**Figure 3B, Table S2**). Despite the presence of these CD8+ T cells in cortical postcapillary venules, FTY720 treated mice failed to develop ECM. Interestingly, PyXL-infected mice with hyperparasitemia exhibited a similar density of CD8+ T cells, 61.0 ± 8.1 cells/mm^2 (**Table S2**), within postcapillary venules (Tukey's test: $T = 1.59$; ns). No CD8+ T cells were detected in the cortical microvasculature of uninfected control mice. Of note, neither the CD8+ T cells remaining after FTY720 treatment of PbA-infected mice nor those found in PyXL-infected mice with hyperparasitemia had any effect on the integrity of the BBB (**Figure 3B**). Thus, it appears that FTY720 treatment prevented a subpopulation of CD8+ T cells from traveling to the brain and that this coincided with the absence of vascular leakage and neurological signs.

Leukocyte accumulation in the entire brain

To elucidate the composition of specific cellular subtypes involved in pathology we quantified leukocytes by flow cytometry in perfused whole brains. In contrast to IVM, no significant difference in CD8+ T cell recruitment was observed between ECM and HP suggesting that flow cytometry may lack the sensitivity to distinguish important focal variations in cellular composition as arrested leukocytes were not observed in other vessels such as capillaries or arterioles.

Overall, significantly more CD45+ leukocytes were found in the brains during ECM compared to hyperparasitemia (23729.3 ± 7573.8 vs. 4483.0 ± 2971.6; ANOVA: $F_{(2)} = 12.42$; $P < 0.001$, Tukey's test: $T = -4.49$; $P < 0.05$) and PbA/FTY720 mice (6059.7 ± 4070.7; Tukey's test: $T = -4.12$; $P < 0.05$) (**Figure 3C, Table S7**). Confirming the IVM data, ECM was associated with the recruitment of significantly higher numbers of Ly6G+ neutrophils than in hyperparasitemia (1470.7 ± 325.5 vs. 518.0 ± 317.2; ANOVA: $F_{(2)} = 9.33$; $P < 0.05$), while there was no significant difference in the number of Ly6C+ monocytes.

The largest increase in cell numbers was observed for F4/80+ macrophages during ECM compared to hyperparasitemia (9648.0 ± 3432.1 vs. 938.0 ± 645.9; ANOVA: $F_{(2)} = 14.35$; $P < 0.01$). Equivalent results were obtained for CD11b+ macrophages (ANOVA: $F_{(2)} = 6.50$; $P < 0.01$). Because total brain leukocytes necessarily contain a large proportion of parenchymal macrophages, we distinguished these from blood-derived macrophages by their low level of CD45 expression [36,56]. When the CD45^{lo}

parenchymal macrophages (microglia) were excluded, the number of the remaining mostly intravascular CD45^{hi} F4/80+ macrophages was significantly higher during ECM compared to PyXL-infected mice (1750.0 ± 285.0 vs. 243.3 ± 171.5; ANOVA: $F_{(2)} = 30.19$; $P < 0.01$) (**Figure 3D**).

FTY720 treatment of PbA-infected mice significantly reduced the number of Ly-6G+ neutrophils (Tukey's Test: $T = -3.69$; $P < 0.05$), and both total and CD45^{hi} F4/80+ macrophages (Tukey's test: $T = -4.31$; $P < 0.05$) in PbA-infected mice so that no significant difference was found for any of the cell types between PbA/FTY720 mice on day 9 and PyXL-infected mice with hyperparasitemia on day 5 (**Figure 3B-D, Table S7**). Equivalent results were obtained for CD11b+ macrophages (**Table S7**). Because neither FTY720-treated PbA-infected mice nor PyXL-infected mice with hyperparasitemia exhibit vascular leakage or neurological signs, it appears that FTY720 prevents BBB opening and the associated leukocyte recruitment, although we cannot exclude that FTY720 affects the brain directly.

ECM-associated changes in leukocyte phenotype

Flow cytometry revealed two distinct leukocyte subsets, namely CD45^{hi} and CD45^{lo} (**Figure 4A**), both of which were significantly more numerous in the brains of PbA-infected mice (ANOVA: $F_{(2)} = 10.38$; $P < 0.05$ and ANOVA: $F_{(2)} = 27.21$; $P < 0.01$, respectively) compared to PyXL-infected mice (Tukey's: $T = -4.45$; $P < 0.05$ and Tukey's test: $T = -7.37$; $P < 0.01$, respectively) (**Table S8**). FTY720 treatment significantly reduced the number of both CD45^{hi} (Tukey's test: $T = -3.08$; $P < 0.05$) and CD45^{lo} (Tukey's test: $T = -3.99$; $P < 0.05$) leukocytes. While the number of CD45^{hi} cells after FTY720 treatment was not statistically different from PyXL infection, the number of CD45^{lo} cells, although significantly decreased compared to PbA infection, remained significantly higher compared to PyXL-infected mice with hyperparasitemia (Tukey's test: $T = -3.38$; $P < 0.05$) (**Table S8**). Significantly more ICAM-1+ (**Table S9**) and CD69+ leukocytes (**Table S10**) were present in the CD45^{hi} and the CD45^{lo} leukocyte subsets from PbA-infected mice compared to PyXL-infected mice (**Figure 4B-D**). FTY720 treatment significantly reduced the number of ICAM-1+, CD69+, and GrB+ leukocytes compared to PbA-infected mice with ECM (**Table S9, S10, and S11**). Further, the CD45^{hi} subset from PbA-infected mouse brains contained consistently higher numbers of ICAM-1+, CD69+, and GrB+ CD8+ T cells compared to PbA/FTY720 mice, although this difference was not statistically significant (**Figure S4A, Table S12**). Furthermore, the median expression levels of ICAM-1, CD69 and GrB in these CD45^{hi} CD8+ T cells were similar amongst PbA-infected, PbA/FTY720, and PyXL-infected mice (**Figure S4B-D**). Likely, the ECM-associated vasculopathy is caused by the high density of activated leukocytes in the postcapillary venules.

PbA   **PyXL**

CD8a

CD4

Gr-1

CD-14

CD-11b
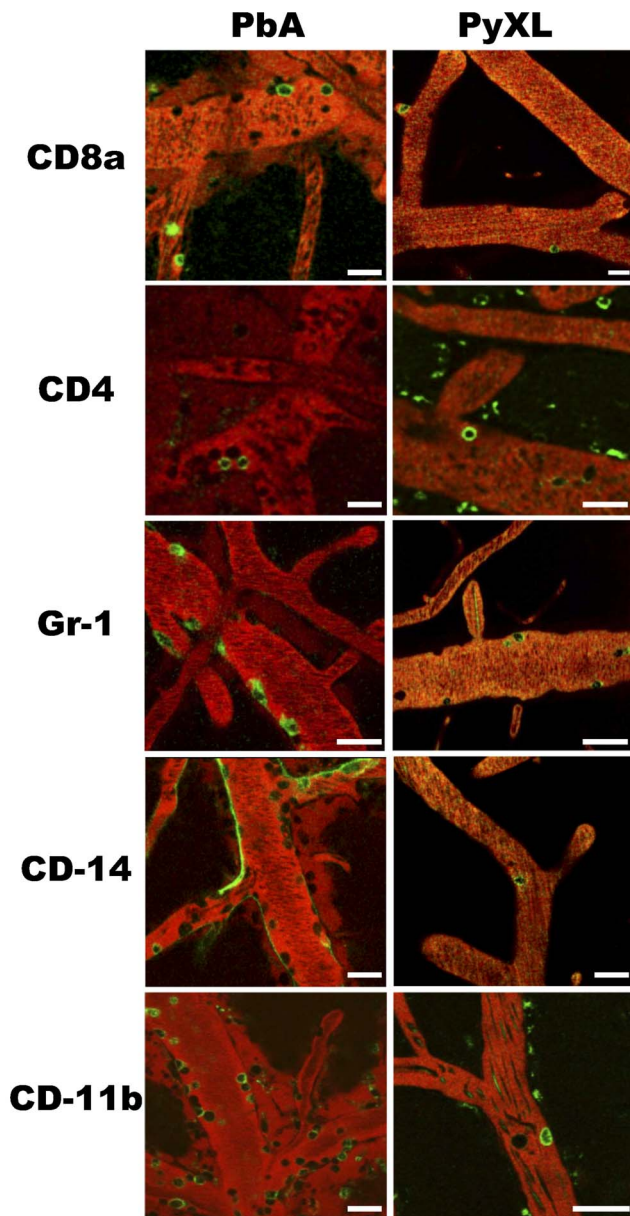
Figure 2. Leukocytes are recruited to cortical postcapillary venules during both ECM and hyperparasitemia. CBA/CaJ mice were infected with PbA, PyXL, or no parasites, subjected to craniotomy at the time of neurological signs or the parasitemia exceeding 50%, and prepared for intravital microscopy. CD8+ T cells, CD4+ T cells, neutrophils, monocytes, and macrophages were labeled by intravenous inoculation of fluorochrome-conjugated mAb (see Materials and Methods for details) and appear as open green circles. The vascular lumen was visualized with Evans blue (red). Representative images from intravital microscopy movies showing arrested green CD8+ T cells (CD8a), CD4+ T cells (CD4), neutrophils (GR-1), monocytes (CD14), and macrophages (CD11b) in postcapillary venules from PbA-infected mice with ECM and PyXL-infected mice with hyperparasitemia. Note that anti-CD14 labels the endothelium (green outline) during ECM in addition to monocytes (open green circles). Scale bars = 20 μm. See **Videos S6–S16** for dynamic information.
doi:10.1371/journal.ppat.1004528.g002

Endothelial activation and expression of adhesion molecules

CD14 and PECAM-1 expression. Next, we explored molecular interactions that could potentially mediate leukocyte arrest to the microvascular endothelium. Various fluorescent markers were intravenously inoculated, which results in immuno-labeling of molecules expressed on or bound to the luminal endothelial surface, while intracellular and extravascular binding sites remain undetected. Previous work indicated that postcapillary venules differ from similarly sized arterioles by differential expression of CD14 and CD31 [21]. PECAM-1 (CD31), generally considered a universal marker of vascular endothelia, was predominantly expressed in arterioles and somewhat less in capillaries. While PECAM-1 was constitutively low in postcapillary venules from infected and uninfected mice, independently of the experimental conditions, CD14 appeared at the time of ECM (day 6–8) on the endothelial surface of postcapillary venules, while capillaries and arterioles were negative [21]. Here we show that surprisingly, CD14 expression in postcapillary venules was not abrogated by FTY720 treatment of PbA-infected mice (**Figure S5, Videos S12 and S16**). In control mice, i.e. PyXL-infected mice with hyperparasitemia (day 5) and uninfected mice, the entire microvasculature including postcapillary venules was consistently CD14-negative (**Figure S5, Video S13**).

ICAM-1 expression on endothelia. Endothelial ICAM-1 plays a role in in leukocyte traversal across the BBB [57] and has been implicated in the pathogenesis of both HCM and ECM [58–62]. Intravenous labeling revealed that ICAM-1 was significantly upregulated (GLM: $F_{(3)} = 154.14$; $P < 0.001$) in postcapillary venules from PbA-infected mice with ECM (**Figure 5A and 5E, Table S13, Video S17**) compared to uninfected control mice (Tukey's Test: T = 19.97; $P < 0.001$) (**Figure 5C and 5E, Table S12**). Interestingly, ICAM-1 upregulation coincided with a labeling pattern that outlined the endothelial junctions. In agreement with earlier reports [63–65], ICAM-1 was also significantly upregulated in postcapillary venules from PyXL-infected mice with hyperparasitemia (**Figure 5B and 5E, Video S18**) compared to uninfected control mice (Tukey's Test: T = 18.79, $P < 0.001$; **Figure 5C, Video S19**). No difference in endothelial ICAM-1 expression was found between PbA-infected mice with ECM and PyXL-infected mice with hyperparasitemia (Tukey's Test: T = −2.05; $P = 0.324$; **Table S13**), which is in agreement with the recruitment of leukocytes to postcapillary venules from both mice with ECM and hyperparasitemia [21]. Surprisingly, however, ICAM-1 was also significantly upregulated in arterioles, both in mice with ECM (Tukey's Test: T = 8.28; $P < 0.001$) and hyperparasitemia (Tukey's Test: T = 4.73; $P < 0.001$) compared to uninfected controls (**Figure 5E, Table S13**), although leukocyte arrest was not observed in this section of the microvascular tree. Further, ICAM-1 was also expressed in postcapillary venules from PbA-infected mice that had been treated with FTY720 (**Figure 5D**). Taken together, these findings do not support a role for endothelial ICAM-1 in ECM pathogenesis.

ICAM-1 expression on leukocytes. In contrast, IVM showed that ECM correlates with ICAM-1 upregulation on leukocytes (**Figure 5A**). The level of ICAM-1 expression per leukocyte was significantly higher (t-test: $T_{(10)} = 2.58$; $P < 0.05$) during ECM (69.2±19.7; day 6–8, 6 mice) compared to hyperparasitemia (48.0±8.9; day 5, 6 mice) (**Figure 5F**). More
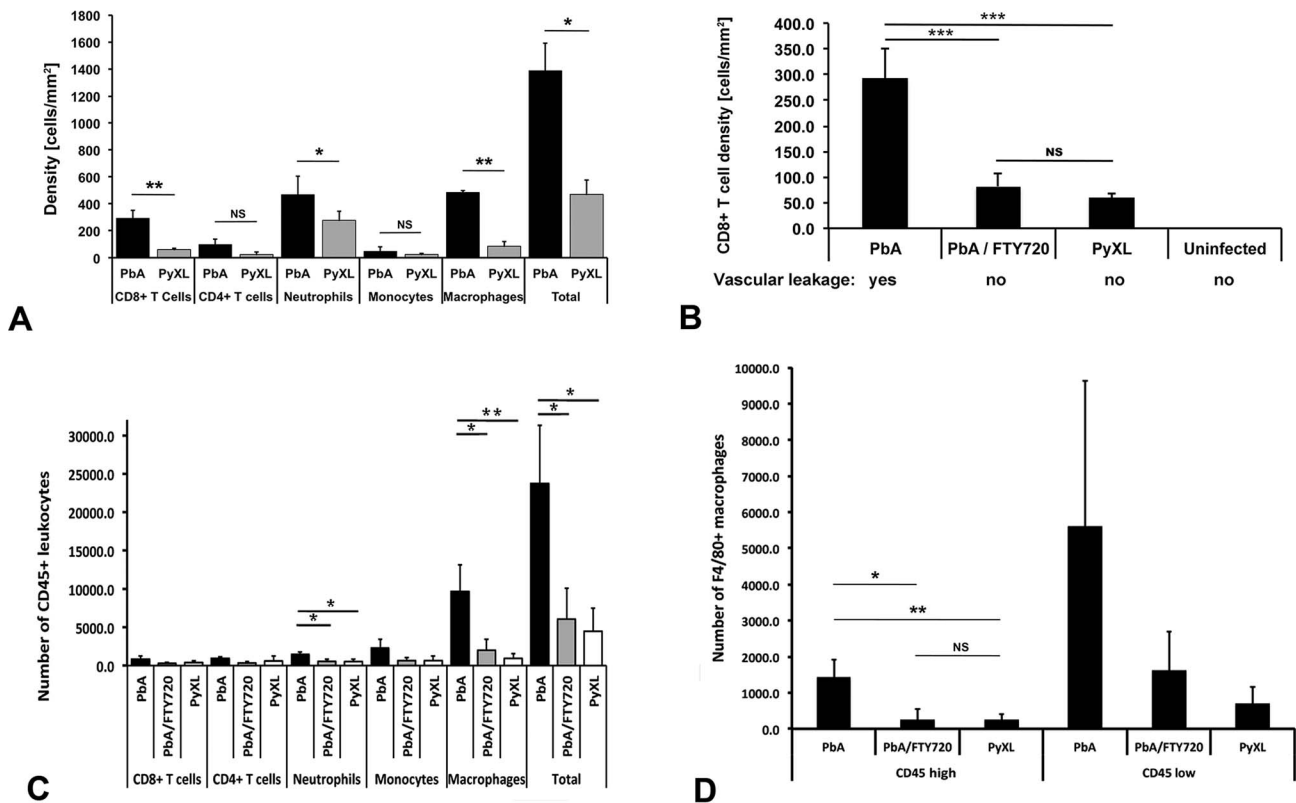
Figure 3. Leukocyte recruitment to cortical postcapillary venules during ECM and hyperparasitemia. A) CBA/CaJ mice were infected with PbA, PyXL, or no parasites, subjected to craniotomy at the time of neurological signs or the parasitemia exceeding 50%, and prepared for intravital microscopy. CD8+ T cells, CD4+ T cells, Gr-1+ neutrophils, CD14+ monocytes, and CD11b+ macrophages were labeled by intravenous inoculation of mAb against CD8+a, CD4+, GR-1, CD14, and CD11b, respectively. Significantly larger numbers of CD8+ T cells, neutrophils and macrophages were found in postcapillary venules from mice with ECM compared to hyperparasitemia ($P<0.05$). The density of CD4+ T cells and monocytes was not significantly different. Most of the arrested leukocytes are macrophages followed by neutrophils, CD8+ T cells, CD4+ T cells, and monocytes. The data represent the mean cell density/mm^2 ± STD. Significance (*, $P<0.05$; **, $P<0.001$) was determined with 1-way ANOVA. See **Tables S2–S6** for details. **B)** Compared to mice with ECM (PbA), significantly less CD8+ T cells are recruited to postcapillary venules from mice with hyperparasitemia (PyXL). Treatment with FTY720 reduces the density of CD8+ T cells to levels similar to those found in PyXL infected mice. No arrested CD8+ T cells were found in the cortical microvasculature from uninfected mice. Vascular leakage was observed in mice with ECM (day 6–8; 76 measurements from 5 mice), but not in FTY720-treated PbA-infected mice (day 8; 19 measurements from 4 mice), PyXL infected mice with hyperparasitemia (day 5; 20 measurements from 6 mice), or uninfected control mice (>10 mice). **C)** Leukocytes were isolated from the brains of PbA-infected (day 6–8), PbA-infected/FTY720-treated (day 9), or PyXL-infected mice (day 5) and analyzed by flow cytometry. Most of the ECM-associated leukocytes are F4/80+ macrophages followed by Ly-6C+ monocytes, Ly-6G+ neutrophils, CD8+ T cells, and CD4+ T cells. Significance (*, $P<0.05$; **, $P<0.01$) was determined with 1-way ANOVA followed by Tukey's test for multiple comparisons. See **Table S7** for details. **D)** FTY720 treatment of PbA-infected mice reduces the number of CD45^{hi} (=blood-derived) macrophages significantly to a level similar to that found in PyXL-infected mice with hyperparasitemia. No significant differences were found for CD45^{lo} (=parenchymal) macrophages. See **Table S7** for details.
doi:10.1371/journal.ppat.1004528.g003

strikingly, the density of ICAM-1 positive leukocytes in postcapillary venules was significantly higher (t-test: $T_{(8)} = 4.30$, $P<0.01$) during ECM compared to hyperparasitemia (**Figure 5G**). Thus, ECM is associated with the arrest of large numbers of ICAM-1+ leukocytes, consistent with a recent report on the contribution of leukocyte ICAM-1 to ECM development [66].

Flow cytometry identified the majority of these ICAM-1+ leukocytes as macrophages (**Figure 6**). Macrophages constituted 65.5% and 54.5% of the ICAM-1+ leukocytes in the PbA and the PbA/FTY720 groups, respectively, but only 32.1% in the PyXL mice. Significantly higher numbers of ICAM-1+ CD45+ macrophages were present during ECM (ANOVA: $F_{(2)} = 13.31$; $P<0.01$) compared to PbA/FTY720 mice (9306.0±3552.2 vs. 1834.3± 1414.9; Tukey's test: $T = -4.76$, $P<0.01$) (**Figure 6B, Table S14**). Interestingly, FTY720 treatment of PbA-infected mice reduced the number of ICAM-1+ F4/80+ macrophages to levels comparable to those found in PyXL-infected mice (656.7±504.1;

Tukey's test: $T = -0.65$, $P = 0.8$; **Figure 6B, Table S14**). Similarly, there was a significant difference in the CD45^{hi} subset of ICAM-1+ F4/80+ macrophages (ANOVA: $F_{(2)} = 30.10$; $P< 0.01$) between PbA-infected and PbA/FTY720 mice (1713.3± 285.3 vs. 365.0±298.2; Tukey's test: $T = -6.45$; $P<0.01$; **Table S14**), i.e. the subset that is comprised mostly of blood-derived macrophages [36,56]. FTY720 treatment of PbA-infected mice reduced the number of ICAM-1+ F4/80+ macrophages in the CD45^{hi} subset to levels similar to those found in PyXL-infected mice (219.0±161.6) so that again, similar numbers were found in the PbA/FTY720 and PyXL-infected groups (Tukey's test: $T = -0.70$, $P = 0.773$; **Table S14**). Equivalent results were obtained for CD11b+ macrophages (**Table S7**). Thus, ECM is associated with 1) the recruitment of large numbers of blood-derived ICAM-1+ macrophages to postcapillary venules and 2) a dramatic increase in the number of ICAM-1+ cells in the parenchyma of the brain, most likely microglia [36,56]. As FTY720 treatment
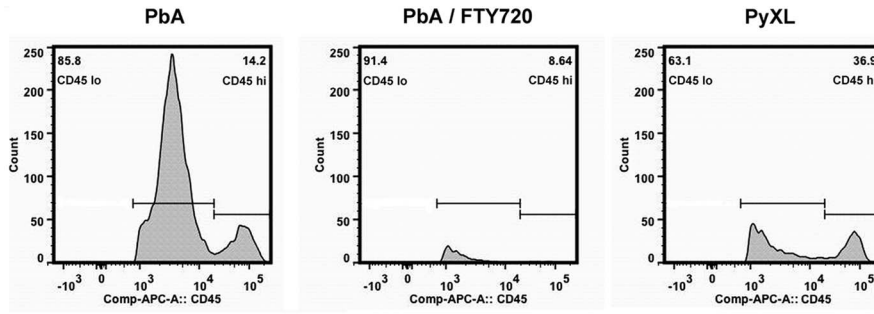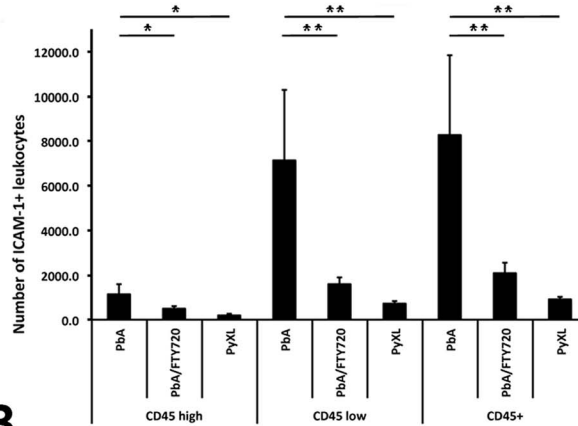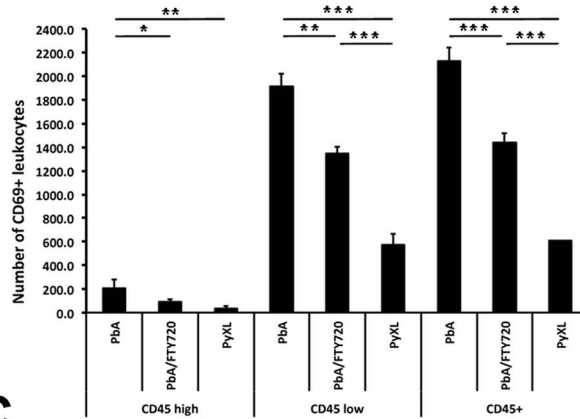
Figure 4. ECM is associated with brain recruitment of CD45+ leukocytes. A) PbA-infected mice exhibit significantly more CD45^hi and CD45^lo leukocytes in the brain compared to PyXL-infected mice. FTY720 treatment of PbA-infected mice reduces the number of CD45^hi and CD45^lo leukocytes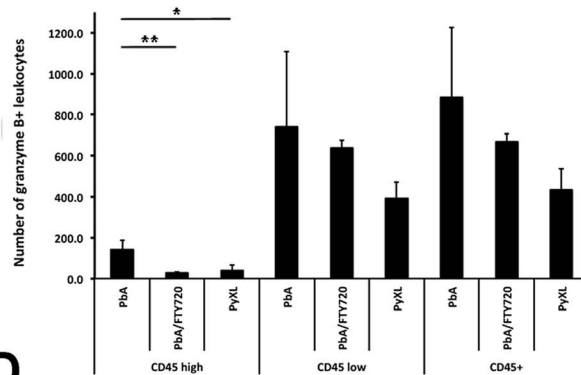 to levels below those observed in PyXL-infected mice. ECM is associated with larger numbers of both CD45^hi and CD45^lo ICAM-1+ (**B**), CD69+ (**C**), and GrB+ (**D**) leukocytes compared to PyXL-infected mice. FTY720 treatment reduces the number of these leukocytes significantly, but not to the level found in PyXL-infected mice. Effect of FTY720 treatment reduces the number of GrB+ CD45^hi leukocytes. The data are based on groups of at least 3 mice per experimental condition. Significance (*, $P<0.05$; **, $P<0.01$) was determined with 1-way ANOVA followed by Tukey's test for multiple comparisons. See **Tables S8–S11** for details.
doi:10.1371/journal.ppat.1004528.g004

prevented this increase in ICAM-1+ macrophages, these data support the idea that the ECM-associated edema has both a vasogenic and a cytotoxic component [17,36].

In agreement with the reported upregulation of ICAM-1 on macrophages under various other inflammatory conditions [67–70], we found higher, albeit statistically not significantly different, levels of ICAM-1 expression on F4/80+ macrophages in PbA-infected mice compared to PyXL-infected mice (4332.6 ± 1007.0 vs. 2560.0 ± 357.7; ANOVA: $F_{(2)}=4.47$; $P=0.05$) (**Figure 6C, Table S15**). Interestingly, FTY720 treatment of PbA-infected mice reduced the level of ICAM-1 expression in F4/80+ macrophages (2606.3 ± 1258.1) resulting in levels similar to those found in PyXL-infected mice (2560.0 ± 357.7). ICAM-1 expression on F4/80+ CD45^lo macrophages was significantly higher in ECM compared to hyperparasitemia (ANOVA: $F_{(2)}=5.57$; $P<0.05$), but no difference in expression level was found between PbA/FTY720 with either ECM or hyperparasitemia infections (Tukey's test: T = $-2.35.24$, $P=0.122$ and T = -0.79, $P=0.720$, respectively). While ICAM-1 expression on F4/80+ CD45^hi macrophages was similar between ECM and hyperparasitemia, a significant difference was observed was between PbA/FTY720 and PyXL-infected mice (ANOVA: $F_{(2)}=5.40$; $P<0.05$). Thus, ECM is associated with a greater number of ICAM-1+ macrophages (**Figure 6B**) and FTY720 treatment prevented this effect. It appears, therefore, that ICAM-1+ macrophages, not endothelia (**Figure 5**), are involved in the ECM-associated vasculopathy.

ECM correlates with platelet arrest and P-selectin deposition in postcapillary venules

P-selectin release from platelet α-granules or endothelial Weibel-Palade bodies promotes the binding of platelets, leukocytes, and plasma proteins to the vascular wall [71–73]. Because both platelet marginalization and P-selectin expression have been implicated in the pathogenesis of both HCM and ECM [18,20–22,74–78], we determined the distribution of this adhesion molecule with respect to arrested platelets in the cortical microvasculature. Upon manifestation of neurological signs, PbA-infected CBA/CaJ mice were inoculated with a PE-conjugated mAb against P-selectin (CD62P), eFluor 450-conjugated anti-CD41 to detect platelets and Evans blue to visualize the vascular lumen [21]. IVM revealed small clusters of marginalized platelets that colocalized with patches of P-selectin on cortical postcapillary venule endothelia (**Figure 7, Video S20**). Occasionally, we observed strings of platelets that appeared to be attached to clusters of platelets (**Video S21**) as has been suggested to occur in HCM based on *in vitro* experiments [79]. In contrast, PyXL-infected mice with hyperparasitemia showed no evidence for P-selectin expression or platelet arrest (**Figure 7, Video S22**). Unlike postcapillary venules, arterioles were consistently negative for P-selectin or arrested platelets, both during ECM and hyperparasitemia. Thus, ECM, but not hyperparasitemia, is associated with marginalization of small numbers of platelets along postcapillary venule endothelia and P-selectin release, either from platelets or endothelia. However, the highly focal nature of both platelet arrest and P-selectin release contrasts with the

uniform endothelial activation as evidenced by CD14 expression, ICAM-1 upregulation, and vascular leakage observed during ECM. Thus, leukocyte arrest is not limited to the P-selectin positive portions of the postcapillary venule endothelia.

Endothelial junction protein expression is unaltered during ECM

FTY720 was previously shown to prevent vascular leakage, neurological signs, and death from ECM [21,39]. To evaluate whether FTY720 protects the BBB by preserving the integrity of endothelial junctions [48,80,81], we determined the expression level of the tight junction (TJ) proteins claudin-5, occludin, and ZO-1 in the cerebral cortex and the cerebellum of 4 PbA-infected mice with ECM (day 6–8), 3 FTY720-treated PbA-infected mice that did not exhibit any neurological signs (day 8 or 9), and 3 PyXL-infected mice with hyperparasitemia (day 5) (**Figure S6 and S7**). Quantification of the fluorescence emission of specific antibodies on 3–4 immunolabeled cryostat sections per experimental condition yielded no significant reduction in protein expression under the different infection and treatment conditions compared to 3 uninfected control mice (**Table S16**). This finding suggests that the TJs remained morphologically intact and supports the hypothesis that the ECM-associated vascular leakage is based on a regulated, potentially reversible, mechanism of BBB opening [21,82].

Thus, comparison of two *Plasmodium* infection models revealed: 1) The venous blood flow impairment during ECM is caused by the arrest of significantly higher numbers of CD8+ T cells, neutrophils, and in particular macrophages in cortical postcapillary venules compared to hyperparasitemia. While a small number of CD8+ T cells and macrophages extravasated into the perivascular space, most of the recruited leukocytes remained intravascular. 2) FTY720 treatment of PbA-infected mice reduced, but did not completely prevent leukocyte accumulation in postcapillary venules, which is consistent with the finding that low numbers of arrested leukocytes are present in PyXL-infected mice with hyperparasitemia without causing vascular leakage or neurological signs. 3) ECM closely correlates with the recruitment of large numbers of ICAM-1 expressing F4/80+ macrophages to the brain. As FTY720 treatment did not reduce the ICAM-1 expression level, the high density of these macrophages in postcapillary venules likely enhances the ECM-associated vascular pathology. 4) Leukocyte recruitment coincides with the onset of neurological signs, but follows BBB opening, as vascular leakage can be observed 1 day prior to symptomatic ECM [21].

Discussion

In this study, we identify a novel key determinant of ECM pathogenesis, namely that leukocyte arrest along the wall of postcapillary venules causes microrheological alterations that severely impair the venous blood flow. Based on our findings, we hypothesize that infection with PbA opens the BBB, which leads to the recruitment of numerous activated CD8+ T cells, ICAM-1+ macrophages, and neutrophils (**Figure 8**). The resulting steric hindrance of the blood flow in postcapillary and larger
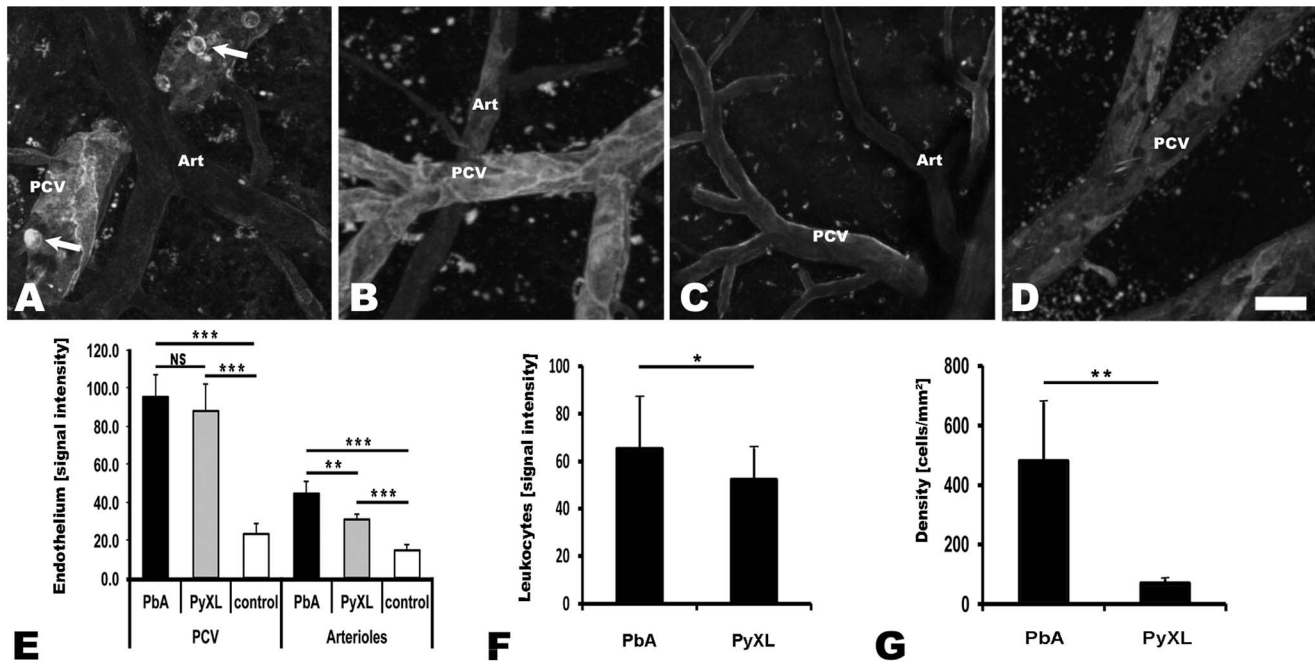
Figure 5. Both ECM and hyperparasitemia are associated with upregulation of endothelial ICAM-1. CBA/CaJ mice were infected with PbA, PyXL, or no parasites (control) and inoculated with PE-conjugated anti-ICAM-1 and Evans blue. **A–D**) Maximum projections of representative intravital microscopy movies showing endothelial ICAM-1 expression in postcapillary venules, and less so in arterioles (Art), in mice infected with PbA and PyXL compared to uninfected control mice. Note the pronounced ICAM-1 label along the endothelial junctions. **A**) PbA-infected mouse with ECM (day 6), **B**) PyXL-infected mouse with hyperparasitemia (day 5), **C**) uninfected control mouse. Note that ECM, but not hyperparasitemia, is associated with the expression of ICAM-1 on the surface of arrested leukocytes (light open circles, arrows). **D**) Endothelial ICAM-1 is upregulated, while ICAM-1 expressing leukocytes are absent, after FTY720 treatment of PbA-infected mice (day 9, no neurological signs). Scale bar = 20 μm. **E**) The endothelial ICAM-1 signal is similarly increased in cortical postcapillary venules from mice infected with PbA and PyXL compared to uninfected control mice. ICAM-1 is significantly upregulated in cortical arterioles during both ECM and hyperparasitemia compared to uninfected control mice. Compared to postcapillary venules, however, the overall level of ICAM-1 expression in arterioles is significantly lower. **F**) ICAM-1 fluorescence emission of individual leukocytes (N = 6) is higher during ECM compared to hyperparasitemia. **G**) The density of ICAM-1 expressing leukocytes in postcapillary venules from mice with ECM is significantly higher compared to mice with hyperparasitemia. Significance (*, $P<0.05$; **, $P<0.01$) was determined with 1-way ANOVA followed by Tukey's test for multiple comparisons. See **Table S13** for details and **Videos S17–S19** for the corresponding dynamic data.
doi:10.1371/journal.ppat.1004528.g005

venules impairs, but does not block, the venous efflux from the brain, which exacerbates the vasogenic edema and causes death as a consequence of intracranial hypertension.

Under physiological conditions, the luminal surface of vascular endothelia is covered with a glycocalix, a 0.5 to >1 μm layer of membrane-bound proteoglycans and glycoproteins that repels RBCs and is critically involved in inflammatory responses, blood coagulation, and blood flow regulation [83–86]. IVM visualizes this glycocalix as a thin red layer, covering arteriolar endothelia from infected and uninfected mice and postcapillary venule endothelia from uninfected control mice. During ECM, the thickness of the RBC-free layer in postcapillary and larger venules was drastically increased. Because the glycocalix typically degrades under inflammatory conditions, leading to exposure of adhesion molecules, leukocyte adhesion, and impairment of endothelial barrier function [85,86], the restriction in the venous blood flow during ECM is likely not caused by components of the glycocalix, but by increasing numbers of arrested leukocytes that prevent RBC from approaching the endothelium. Although the functional cross-section of postcapillary venules was occasionally reduced by more than 80%, complete vascular obstruction was not observed. These findings argue in favor of a combined vascular sequestration and immuno-pathological etiology of ECM [87–89].

The reduction in the venous blood flow must be expected to have major consequences for the physiology of the brain. First,

the overall hypoperfusion of the brain, enhanced by inadequate contact between RBCs and the endothelium, likely contributes to the drastically reduced O_2 delivery to the cerebral parenchyma observed in ECM-susceptible C57BL/6 mice [90]. In addition, by increasing the wall shear stress, leukocyte adhesion is expected to reduce the blood volume flow in postcapillary venules dramatically [91]. Finally, a reduction of the venous efflux from the skull, caused by a generalized narrowing of the lumen of venous microvessels, necessarily increases the intracranial pressure. The finding that brains from mice with ECM, but not hyperparasitemia, are swollen and spongy and bulge out of the skull, if the Dura mater is accidentally damaged during craniotomy clearly documents the dramatically increased intracranial pressure during the agonal phase of the disease. The reduced venous efflux from the brain may exacerbate vascular leakage, brain edema, and hemorrhages - cerebral alterations that are also associated with HCM [92]. Brain swelling and edema is extremely common in adult HCM on CT scan [93,94]. Increased intracranial pressure has long been associated with poor prognosis and neurological sequelae in severe pediatric HCM [50,95–98]. In fact, recent longitudinal MRI observations in Malawian children have identified intracranial hypertension as the single most important MRI finding associated with HCM development and the most reliable predictor of death [54,99].
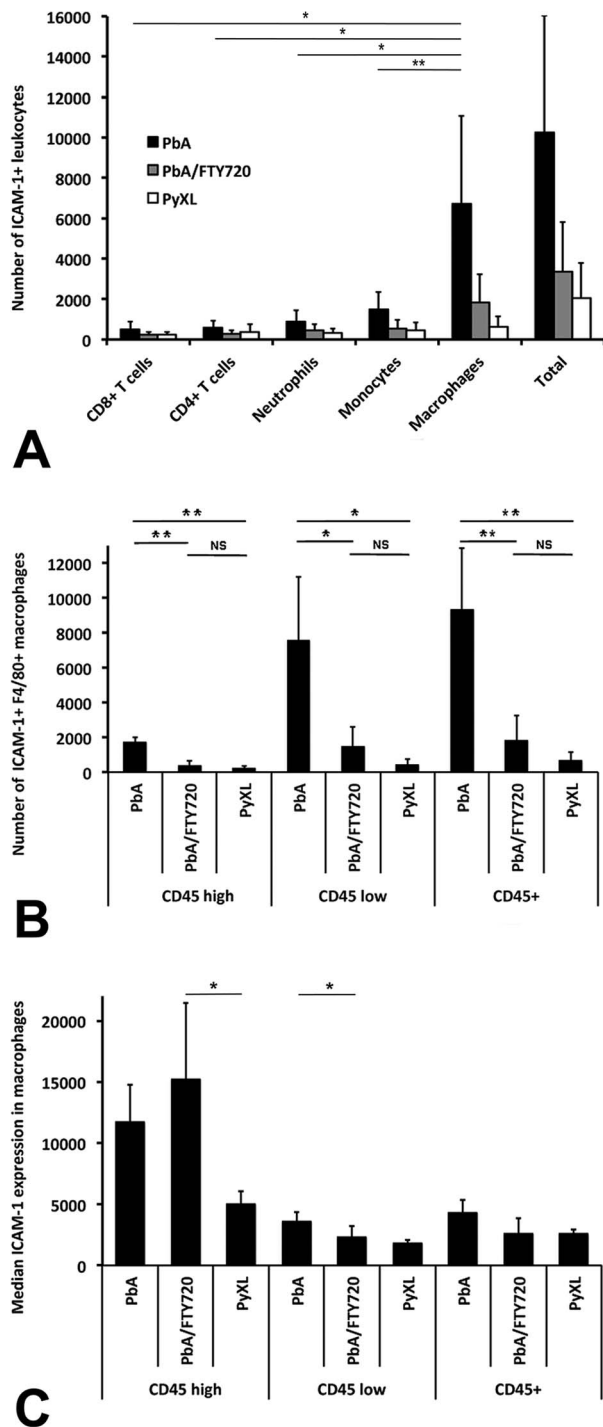
Figure 6. ECM is associated with the recruitment of ICAM-1+ macrophages. Leukocytes were isolated from PbA-infected, PbA-infected/FTY720-treated, or PyXL-infected mice and subjected to flow cytometric analysis. **A**) The vast majority of ICAM-1+ leukocytes are macrophages, which were identified with mAb F4/80. **B**) FTY720 treatment reduces the number of ICAM-1 macrophages to levels similar to those found in PyXL-infected mice. **C**) No significant difference was found for the median ICAM-1 expression levels in macrophages from PbA-infected versus PbA-infected/FTY720-treated mice. Significance (*, $P<0.05$; **, $P<0.01$) was determined with 1-way ANOVA followed by Tukey's test for multiple comparisons. See **Table S14 and S15** for details.

doi:10.1371/journal.ppat.1004528.g006

PbA-infected mice also exhibit arteriolar vasospasms during the final stage of ECM [100] and it has been suggested that the reduction in the cerebral blood flow observed by MRI [101] is due to increased production of vasoconstrictive factors or inhibition of vasodilating mediators [102]. Subsequent work [103,104] revealed that endothelin-1 (ET-1), a potent vasoactive peptide with inflammatory and platelet-activating properties [105–108], is upregulated during both ECM and HCM [109–112]. Indeed, the arteriolar vasoconstrictive effect of ET-1 could be responsible for ECM induction in the PbA-infected C57BL/6 mouse model [108], because injection of exogenous ET-1 induces neurological signs in PbNK65-infected mice, which normally do not develop ECM [113], and because blockage of the ET-1 receptor A prevents ECM development in PbA-infected mice [110]. However, ET-1 has a plasma half-life of well under one minute in rodents [114] so that vasoconstriction alone cannot explain the increased intracranial pressure observed during ECM. Because ET-1 also stimulates endothelial activation with upregulation of adhesion molecules, promotes leukocyte adhesion, and increases vascular permeability [105,106], there is a possibility that ET-1 induces ECM by restricting the venous blood flow. Similarly, administration of nitric oxide (NO), a key messenger involved in regulation of platelet adhesion and inflammatory and immune responses [115], decreased both leukocyte accumulation and vascular resistance in larger venules of PbA-infected mice [78,116–121]. We conclude that the ultimate cause of death from ECM is a combination of arteriolar vasoconstriction and severe reduction in the blood efflux from the brain due to leukocyte adhesion in the venous microvasculature.

Compared to PyXL-infected mice with hyperparasitemia, PbA infection triggered the recruitment of significantly more CD8+ T cells to postcapillary venules at the time of, but not prior to, ECM development. Together with the finding that CD8+ T cells were absent in mice that survived the critical time for ECM development, these data suggest that neurological signs and T cell recruitment are correlated and occur rapidly. CD8+ T cells from C57BL/6 mice immunized with PyXNL can confer protection against lethal PyXL infection [122], whereas CD8+ T cell accumulation in the brain of PbA-infected C57BL/6 mice was abolished and the mice were completely protected from ECM when co-infected with *P. yoelii* [123,124]. However, similar numbers of CD8+ T cells accumulated in the brains of PbA-infected C57BL/6 mice with ECM and PbNK65-infected mice without neurological signs [34], further supporting the notion that ECM-eliciting parasites such as PbA induce the recruitment of a qualitatively different CD8+ T cell population to the brain.

FTY720 treatment decreased the number of CD8+ T cells to levels similar to those found in PyXL-infected mice. Despite the presence of the remaining CD8+ T cells, neither FTY720-treated PbA-infected mice nor PyXL-infected mice developed neurological signs. A small percentage of CD8+ T cells entered the perivascular space during ECM, but not hyperparasitemia. This could be explained by upregulation of the leukocyte common antigen CD45, because CD45 expression is typically enhanced in response to stress signals, leading to increased leukocyte motility [125] and brain infiltration, for example after seizure [126]. ECM coincided with larger numbers of CD8+ T cells expressing CD69, one of the earliest lymphocyte activation markers [127,128], and FTY720 treatment reduced the number of CD69+ CD8+ T cells to levels similar to those found during hyperparasitemia. Previous work supports a correlation between ECM and CD69+ CD8+ T cells: 1) Recruitment and activation of CD8+ T cells and CD69 expression were reduced in ECM-resistant mice [129]. 2) Peripheral CD8+ T cells were predominantly CD69+ during
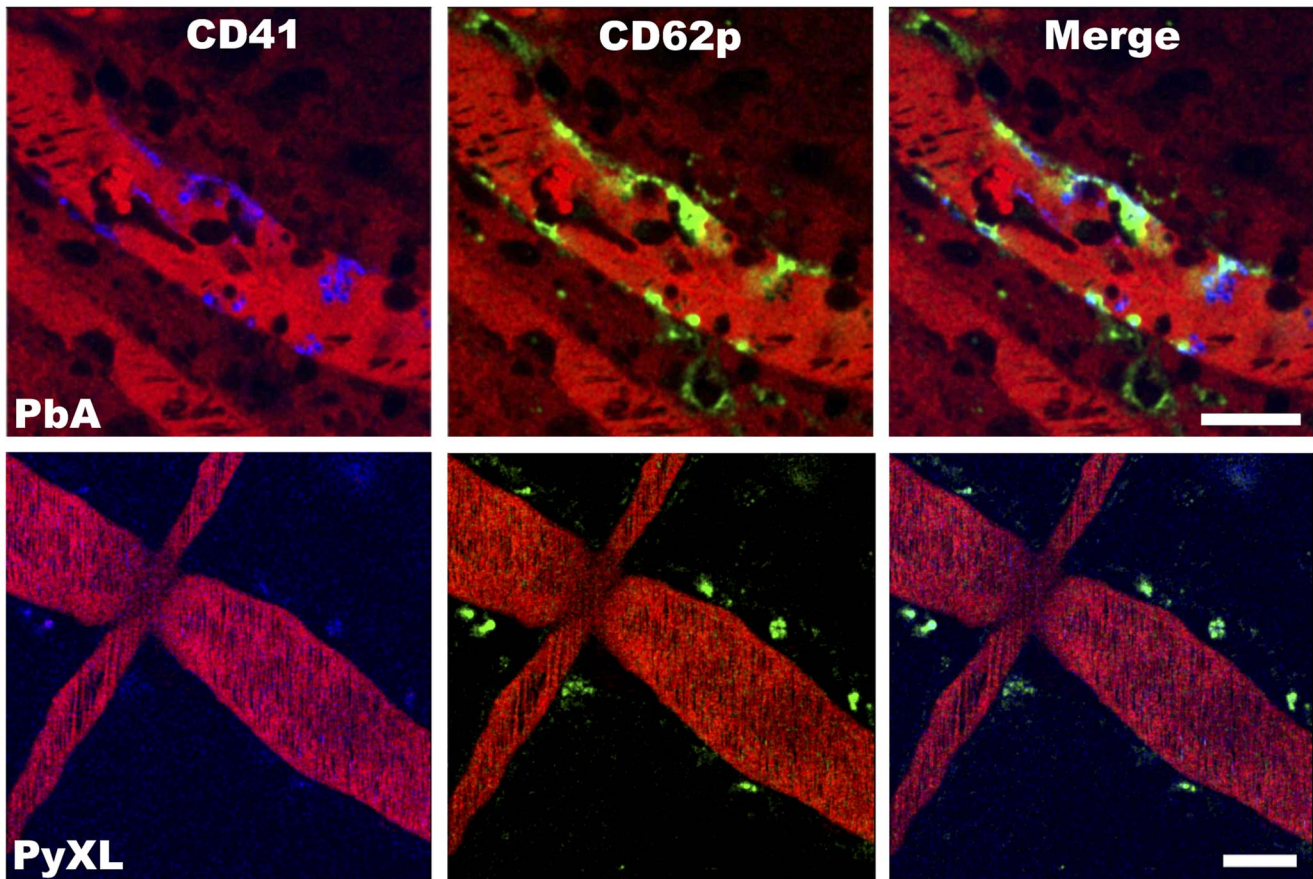
Figure 7. ECM correlates with the arrest of P-selectin expressing platelets in postcapillary venules. PbA-infected mice exhibit small clusters of CD41+ platelets (blue) and patches of P-selectin (green) along the wall of postcapillary venules at the time of ECM. Platelets remained in circulation and P-selectin was not detected in postcapillary venules from PyXL-infected mice with hyperparasitemia. The vascular lumen is visualized with Evans blue (bright red). Note that Evans blue has leaked into the brain parenchyma of the PbA-infected mouse (dark red shade on either side of the postcapillary venule). Scale bars = 50 μm. See **Video S20 and 22** for the corresponding dynamic data.
doi:10.1371/journal.ppat.1004528.g007

ECM and expressed the phenotype of memory T cells [130]. 3) The ECM-associated upregulation of CD69 was reversed and disease was prevented by interference with the angiotensin I pathway [131]. 4) Ghanaian *P. falciparum* infected pediatric patients with clinical HCM or severe anemia showed similar T cell activation profiles with a significantly increased frequency of CD69+ cells compared to asymptomatic children [132]. The median expression levels per cell of CD69 and GrB did not differ between the experimental groups suggesting that ECM pathogenesis correlates with a high density of CD69+ and GrB+ CD45^{hi} CD8+ T cells in postcapillary venules. FTY720 treatment of PbA-infected mice reduced the number of CD4+ T cells to levels similar to those observed for PyXL-infected mice. Together, these data suggest that FTY720 treatment prevents ECM by inhibiting the trafficking of activated CD8+ and CD4+ T cells to the brain.

FTY720 treatment of PbA-infected mice also reduced the number of macrophages and neutrophils to levels similar to those found in the brains of PyXL-infected mice, supporting the notion that these leukocytes exacerbate edema formation during ECM [26,27]. Of particular importance, FTY720 treatment prevented the recruitment of large numbers of ICAM-1+ macrophages to the brains of PbA-infected mice. This finding sheds light on an unexpected new role of ICAM-1 in the pathogenesis of ECM. While FTY720 may preserve the integrity of the BBB primarily by preventing leukocyte recruitment to the brain, activated platelets

release phosphorylated FTY720 [133,134], which acts as a full agonist on the endothelial S1P receptor S1PR4; therefore, FTY720 may prevent the ECM-associated vascular leakage by strengthening the endothelial actin cytoskeleton [135,136]. Further, FTY720 may regulate endothelial barrier function by directly modulating endothelial junction tightness, because the increased vascular leakage observed in mice deficient in plasma S1P can be reversed by restoring plasma S1P levels [47,48,80,81]. This finding may explain why FTY720 administration must be started prior to the onset of vascular leakage [21,39] and why attempts to rescue mice with symptomatic ECM, when leukocyte recruitment was already in progress, were unsuccessful (A. Movila and U. Frevert, unpublished observations). Further, FTY720 can cross the BBB and may thus be able to directly modulate parenchymal cells by interacting with S1P receptors in the CNS. The resulting feedback from the CNS on the activation status of the BBB may in turn alter the interaction with the immune cells. Future testing of FTY720 or related compounds in the ECM model is expected to reveal more detail on the exact mechanism of BBB opening and vascular inflammation in ECM. The ECM model may also improve our understanding of the pathogenesis of HCM. Ugandan, Malawian, and Central Indian children with HCM exhibit decreased S1P plasma levels compared to those with uncomplicated malaria and a low angiotensin-1 to angiotensin-2 plasma ratio discriminates HCM and severe non-cerebral from uncomplicated malaria and
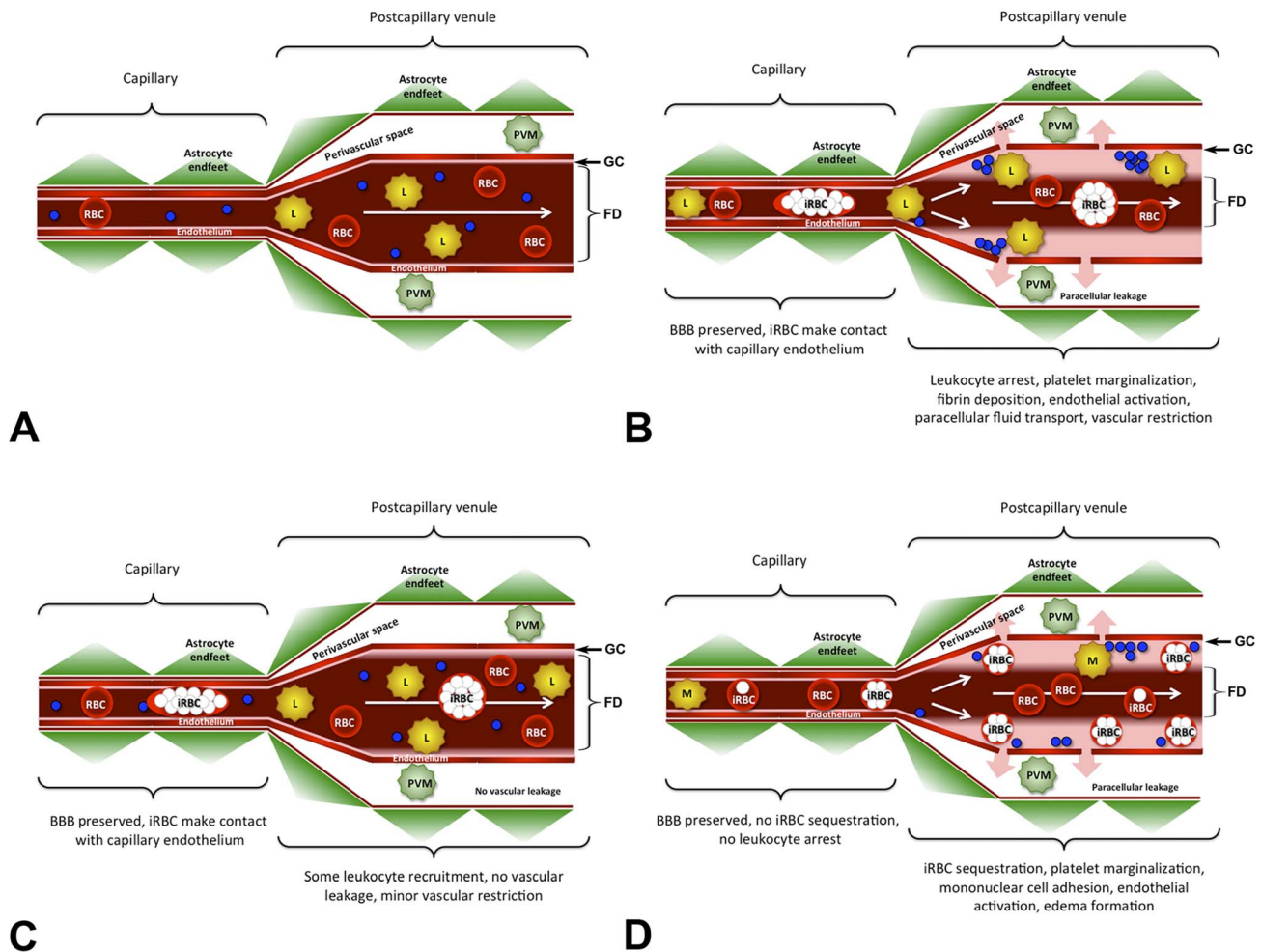
Figure 8. Model for the ECM-associated venous blood flow restriction. A) Under normal conditions, blood passes through the cerebral microvasculature without leukocytes arresting in postcapillary venules. Except for the narrow glycocalix (GC) lining the vascular endothelium, the entire vascular diameter is used for the bloodstream, the functional diameter (FD) is not restricted, and the BBB is intact. **B)** Infection with PbA causes endothelial junction opening at the BBB in the absence of junction protein degradation or endothelial death. During ECM, arrested leukocytes form steric obstacles that reduce the functional diameter (FD) of postcapillary venules resulting in a severe restriction of the venous blood flow. As a consequence, the paracellular leakage of plasma into the PVS (pink arrows) is exacerbated. Like uninfected RBC, iRBC travel with the bloodstream and do not arrest. **C)** During hyperparasitemia, significantly fewer leukocytes and no platelets adhere to the postcapillary venule endothelium compared to ECM. Consequently, the restriction in the venous blood flow is minor and there is no vascular leakage. **D)** Hypothetical model for pediatric *P. falciparum* HCM. While leukocytes, RBC, and all iRBC pass through capillaries without adhering to the endothelium, late-stage iRBC, mononuclear cells, and platelets sequester on the wall of postcapillary venules thus restricting the venous blood flow and exacerbating the leakage of plasma into the perivascular space. Because of the significant reduction in the functional diameter (FD) of the postcapillary venule, ring-stage iRBC, uninfected RBC, and most leukocytes must flow through the center of the vessel. The arterial blood flow remained unaffected under all experimental conditions. PVM = perivascular macrophage, iRBC = infected red blood cell, L = leukocyte, M = mononuclear cell, blue circles = platelets.
doi:10.1371/journal.ppat.1004528.g008

also predicts mortality from HCM [39,137–140]. As these reports strongly suggest the involvement of the S1P pathway HCM, screening for novel immunomodulatory drugs and exploration of their endothelial barrier-promoting effects is warranted.

We observed significantly more neutrophils in postcapillary venules and whole brain during ECM compared to hyperparasitemia. Considering that the role of neutrophils in the pathogenesis of CM is understudied to date, this finding is of particular interest. FTY720 treatment of PbA-infected mice reduced the number of neutrophils significantly so that levels similar to those found during hyperparasitemia were reached, which supports the previously suggested involvement of neutrophils in the ECM-associated vasculopathy and edema formation [26,141].

The number of arrested monocytes was increased similarly in PbA- and PyXL-infected mice compared to uninfected control mice suggesting that monocyte recruitment correlates with *Plasmodium* infection in general, not ECM in particular. This finding is in agreement with earlier reports showing that monocytes are not involved in iRBC accumulation in the brain at the time of ECM [26,27]. Intravenous injection of fluorescent anti-CD14 revealed that monocytes were generally confined to the vascular lumen, although we occasionally detected labeled monocytes in the Virchow-Robin space. Similarly, intravenous injection of the macrophage marker anti-CD11b resulted in labeling of PVM. Because part of the PVM population derives from blood monocytes [53], these fluorescent monocytes may have

been labeled before extravasating to replenish the pool of PVM in the perivascular space.

Flow cytometric measurement of leukocyte recruitment to the brain essentially corroborated our IVM findings suggesting that the cortical microvasculature reflects the ECM-associated pathological events in the entire brain. A few conceptual differences between IVM and flow cytometry are noteworthy. First, IVM confirmed the notion that the healthy murine brain has an extremely low level of immune surveillance with the almost complete absence of T cells, neutrophils, monocytes, and B cells [21,142]. Expression of adhesion molecules is low on the healthy human postcapillary venule endothelium, and upregulation of P-selectin, E-selectin, ICAM-1, and VCAM-1 contributes to the pathogenesis of HCM [53,58,143]. Second, IVM provides information on the location of recruited leukocytes and their dynamics with respect to the complex and heterogeneous microvascular network of the brain. Third, intravenous labeling generally visualizes only intravascular leukocytes including those that extravasate between marker injection and imaging. However, the BBB at the level of postcapillary venules is naturally leaky, i.e. it allows passage of macromolecules including immunoglobulins into the Virchow-Robin space [38]. During ECM, this barrier becomes even more permeable, which makes distinction of recently extravasated from resident perivascular cells difficult. While CD8+ T cells do not patrol the cerebral microvasculature of uninfected mice and are therefore unlikely to extravasate into the perivascular space of naïve mice, the fluorescent CD11b+ macrophages we found in the perivascular space of mice with ECM could either have been labeled intravascularly and then extravasated or they could have been labeled after entering the perivascular space due to diffusion of the cell-specific markers across the BBB. Thus, while the majority of leukocytes remain confined to the vascular lumen during ECM, a small number of CD8+ T cells and possibly CD11b+ macrophages extravasate into the perivascular space. Fourth, flow cytometric measurement of the expression level of CD45 allowed distinction between blood-derived and parenchymal macrophages [56]. Using this approach, we found that ECM is associated not only with significantly higher numbers of ICAM-1+ CD45^{hi} (= blood-derived) macrophages, but also ICAM-1+ CD45^{lo} (= parenchymal) macrophages compared to mice with hyperparasitemia and FTY720-treated PbA-infected mice. Together with the ECM-associated activation of microglia [144] and the enhanced expression of CCR5 on non-hematopoietic cells [145], ICAM-1 upregulation on both blood-derived and parenchymal macrophages supports the notion of a mixed vasogenic and cytotoxic nature of the edema in ECM [17,146]. Finally, IVM was critical to visualize endothelial activation markers within defined parts of the microvascular tree. Thus, IVM and flow cytometry provided highly complementary results.

BBB opening in the young CBA/CaJ mice used here begins at least one day prior to the onset of neurological signs, while leukocyte recruitment to the brain occurs only afterwards [21]. In 129,B6 mice, neither antibody-mediated neutrophil depletion nor clodronate-mediated macrophage depletion, done 1 or 2 days prior to ECM development, respectively, prevented neurological signs [26,145]. While this was interpreted as neutrophils and macrophages not being involved in ECM development, an alternative explanation is that the BBB was already leaky at this late time point and the resulting vasogenic edema had already caused microglial activation. Clodronate liposomes do not cross the BBB [147–149] so that the microglia was likely unaffected and the resulting cytotoxic edema not prevented in these studies. Further, depletion of macrophages and granulocytes by adminis-

tration of AP20187 to MAFIA mice on days 5, 6, and 7 after infection resulted in a >80% reduction of these cells in the blood [27,150]. Again, as AP20187 does not cross the BBB [151], ECM development likely manifested because the activated microglia was not eliminated. Importantly, CD8+ T cells alone failed to induce any of the typical signs of ECM including convulsions and death without the direct neurotoxic effect of intravenously administered folic acid [26,145]. Thus, it appears that both hematogenic and parenchymal macrophages play a role of in the pathogenesis of ECM. A more recent study in C57BL/6 mice emphasizes the crucial role of monocytes/macrophages in lymphocyte recruitment to the brain. Clodronate treatment 2 days prior to manifestation of neurological signs reduced the recruitment of CD8+ T cells, CD4+ T cells, and NK cells to the brain 2.8-fold, 1.8-fold, and 4.6-fold, respectively, and failed to alter the course of disease development [152]. Clodronate treatment 2 days prior to infection with PbA, on the other hand, prevented ECM development [152]. Thus, the exact mechanism by which blood-derived macrophages contribute to disease development needs further and more specific investigation. Taken together, these data suggest the following scenario: PbA infection induces BBB opening, which results in vasogenic edema and microglial activation. The ensuing cytotoxic edema then leads to endothelial activation with recruitment of leukocytes that in concert restrict the venous blood flow, which further weakens the already impaired BBB. Eventually, these events culminate in the typical irreversible damage associated with fatal malarial encephalopathy. However, the differential progression of the vasogenic versus the cytotoxic edema and their relative contribution to brainstem compression and death clearly require further experimental attention.

The critical role of ICAM-1 in the pathogenesis of severe *P. falciparum* malaria and the binding of *P. falciparum* iRBC to the endothelium is generally accepted [59,61,153–159]. However, comparison of the endothelial ICAM-1 expression levels in the brains of *P. falciparum* versus *P. vivax* infected individuals is necessary to determine whether or not HCM correlates with upregulation of ICAM-1 in postcapillary venules. ICAM-1 upregulation has also been implicated in the pathogenesis of ECM [63,77,78,160–162]. While the cellular origin of ICAM-1 was not determined, treatment of PbA-infected mice with NO reduced ICAM-1 upregulation in the brain along with leukocyte sequestration and vascular leakage [78]. We show that upregulation of endothelial ICAM-1 correlates with *Plasmodium* infection in general, not with ECM in particular. Because ICAM-1 upregulation was not observed in mice deficient in RAG-1 or IFN-γ on day 6 after infection with PbA [163], the Th1 type cytokines IFN-γ and lymphotoxin, in synergy with TNF from macrophages [163,164], may induce ICAM-1 expression throughout the brain microvasculature of ECM-susceptible mice, both during ECM and hyperparasitemia. Together with the finding that FTY720 treatment of PbA-infected mice does not prevent ICAM-1 upregulation in postcapillary venules, these data argue against a role of this endothelial adhesion molecule in the pathogenesis of ECM.

CD14 appeared on the surface of postcapillary venule endothelia selectively at the time of neurological signs (day 6–8), which is in agreement with the well-known involvement of CD14 in endothelial activation, neuroinflammation, and leukocyte recruitment to the cerebral microvasculature [165–168] and the finding that CD14-deficient mice are protected against ECM [169]. Further, because CD14 plays an important role in the non-phlogistic clearance of apoptotic cells [170], its expression on postcapillary venule endothelia may reflect the well-documented

increase in apoptosis during ECM [171–173]. Interestingly, malaria-associated microparticles carry phosphatidylserine on their surface [174]. Because the plasma levels of endothelial, platelet, and erythrocytic microparticles increase at the onset of the ECM-associated neurological signs [175], CD14 may be involved in the recruitment of microparticles to postcapillary venule endothelia. Platelet-derived microparticles are known to promote macrophage differentiation [176] and may contribute to the observed upregulation of ICAM-1 on the macrophage surface.

We show that ECM occurs without apparent physical degradation of endothelial TJs, measurable loss of claudin-5, occludin, and ZO-1 and in the absence of endothelial death [21]. Together, these findings argue against widespread and irreversible endothelial injury, for example due to cytotoxic T cell-mediated apoptosis or long-lasting vascular occlusion [177], as a major pathogenetic mechanism leading to malarial coma and death [82,88,178,179]. Instead, and in agreement with the observation that ECM-susceptible mice can be rescued by anti-LFA-1 treatment even minutes before imminent death [180,181], the preserved TJ integrity suggests that BBB opening during ECM is under the control of a regulated mechanism [21,82,182]. In support of this notion, fast-acting anti-malarial drugs can prevent ECM one day before the expected onset of neurological signs, although CD8+ T cells still accumulate in the brain [32,34].

Platelets play a crucial role in the early stages of the pathogenetic cascade of ECM [9,183,184]. Blockage of platelet activation or shedding of platelet-derived microparticles confers resistance to ECM [13,22,160,184]. At the time of ECM, platelets arrest focally and in small numbers in the cortical microvasculature [21] where they closely associate with P-selectin positive areas on postcapillary venule endothelia, confirming the reported involvement of both platelets [18,20–22,74–76] and P-selectin [77,78] in the pathogenesis of HCM and ECM. Although platelets produce many factors including VEGF, ROS, and thrombin that are able to directly impair endothelial barrier function [185], the highly focal nature of platelet arrest [20,21] is difficult to reconcile with the homogenous vascular leakage throughout the entire venous microvasculature at the time of ECM [21]. In agreement with their crucial role early in the pathogenesis of ECM, platelets are more likely to accomplish their vascular permeability-augmenting effect indirectly, namely by 1) facilitating leukocyte arrest in postcapillary venules [22,57,186,187], 2) boosting ROS formation in leukocytes [185], and 3) enhancing cytokine secretion and cytotoxic capacity of effector T cells [188]. Thus, platelets adhering to small foci of endothelial P-selectin may serve as early nucleation points for the gradually spreading, cytokine-induced vasculopathy observed in postcapillary venules from ECM-susceptible mice.

In conclusion, we find that steric hindrance, mediated by large numbers of arrested CD8+ T cells, macrophages, and neutrophils in postcapillary venules, causes a severe restriction in the venous blood flow. Based on this observation, we hypothesize that completely different pathogenetic mechanisms - cytoadherence of P. falciparum iRBC in HCM and sequestration of leukocytes in ECM - can result in the same pathophysiological outcome: a severe reduction in the blood efflux from the brain. If the resulting increase in intracranial pressure intensifies the cerebral edema to the point of brainstem herniation, then compression of the respiration centers in pons and medulla could cause death by respiratory arrest.

Intracranial hypertension is a known risk factor for poor outcome in pediatric HCM [189,190], but how this leads to neural injury is unknown [191,192]. As discussed in a recent review [193], intracranial hypertension eliminates the need to explain any

selective recognition mechanism Plasmodium might use to target multiple sensitive sites in the brain [194]. Intracranial hypertension leading to general swelling and hypoperfusion of the brain can also explain all of the neurological sequelae in HCM survivors [194]. Reports associating loss of smell, deafness, and blindness with both HCM and ECM support the notion that sequestration of iRBC as well as leukocytes can cause intracranial hypertension [192,195–200]. Further, leukocyte sequestration is likely also involved in intracranial hypertension during P. falciparum HCM, as artesunate treatment was more efficacious in Asian adults compared to African children with more mononuclear cell accumulation [157,201,202] and also failed to rescue HCM patients with a low parasite biomass in the brain [203]. Thus, HCM and ECM induce very similar neurological symptoms and sequelae.

Thus, despite fundamental differences in parasite biology, the non-cytoadherent rodent parasite PbA could be used as a model to better understand how rheological alterations might lead to the annual death from HCM of over half a million people [204]. Perhaps more importantly, venous efflux disturbances due to leukocyte sequestration could also explain the cerebral complications that are increasingly reported for severe infections with P. vivax, another knobless (essentially non-cytoadherent) Plasmodium species [205–214]. The marked proinflammatory responses and reversible microvascular dysfunction associated with P. vivax infections [215,216], together with the shared propensity for reticulocyte invasion [217–220], may render the PbA-infected mouse model suitable for study of the pathogenesis of severe P. vivax malaria. Hence, this model promises to shed light on the ultimate cause(s) of death from cerebral malaria.

Materials and Methods

Ethics statement

This study was conducted in strict accordance with the recommendations in the Guide for the Care and Use of Laboratory Animals of the National Institutes of Health. The protocol was approved by the Institutional Animal Care and Use Committee, NYU School of Medicine (Protocol number 101201-01). All surgery was performed under ketamine-xylazine-acepromazine anesthesia, and all efforts were made to minimize suffering.

Parasites

P. berghei and P. yoelii parasites were maintained by passage through female Anopheles stephensi mosquitoes [221]. The green fluorescent P. berghei ANKA strain (PbA-GFP) was a kind gift from Dr. Andy Waters, University of Glasgow, UK [222]. The lethal P. yoelii strain 17XL, originally derived from the non-lethal 17X strain [223], was kindly provided by Dr. James Burns (Drexel University College of Medicine) [224,225]. WT PyXL were transfected to express RedStar, an improved version of the red fluorescent protein drFP583/DsRed/RFP [226], under the control of the elongation factor 1α promoter using a novel replacement strategy [21,227,228] and termed PyXL-RFP [21]. Both PbA-GFP and PyXL-RFP emit fluorescence throughout the entire life cycle.

Mice and infection

Mice were CBA/CaJ (Jackson Laboratory, Bar Harbor, ME). Animals were maintained and used in accordance with recommendations in the guide for the Care and Use of Laboratory Animals. CBA/CaJ mice were infected at the age of 3 weeks (body weight of 12–15 g) by intraperitoneal injection of 0.5–10×10^6

iRBC as described [21]. In our hands, 3 week-old CBA/CaJ mice responded to PbA infection with neurological signs and died from ECM comparable to adult mice used by others [3,6,18,22,23, 76,141,169,229–244]. The parasitemia was monitored daily using Giemsa stained blood smears and mice were sacrificed upon development of ECM or hyperparasitemia.

Assessment of neurological signs

PbA-infected mice were considered ECM positive when two or more parameters clearly indicated behavioral alteration including body position, spontaneous activity, startle response, tremor, gait, touch escape, and righting reflex [245]. Quantitative assessment of ECM-associated neurological signs was performed using the Rapid Murine Coma and Behavior Scale (RMCBS) with values of 3–7 defined here as severe, 8–16 as mild, and 17–20 as no ECM [246]. PyXL-*infected* mice exhibited a hunched position, pale skin color, and an increased respiration rate when parasitemia levels reached levels around 80%, but failed to present typical neurological manifestations.

FTY720 treatment

For IVM, groups of 15 PbA-infected CBA/CaJ mice received one daily oral dose of 0.3 mg/kg FTY720 starting one day before infection or no treatment as described [21,39]. At the onset of neurological signs, mice were injected with Evans blue and examined by IVM. Mice surviving the critical period of ECM development were inoculated with Evans blue and PE-conjugated species anti-species CD8a and imaged on day 9. Groups of 5 PyXL-infected or uninfected mice were inoculated with the same markers and imaged on day 5 for comparison. For flow cytometry, PbA-infected mice, FTY720-treated PbA-infected mice, and PyXL-infected mice were analyzed on day 6–8, day 8, and day 5, respectively.

Anesthesia, craniotomy, and intravital microscopy

Mice were anesthetized by intraperitoneal injection of a cocktail of 50 mg/kg ketamine (Ketaset, Fort Dodge Animal Health, Fort Dodge, IO), 10 mg/kg xylazine (Rompun, Bayer, Shawnee Mission, KS), and 1.7 mg/kg acepromazine (Boehringer Ingelheim Vetmedica, St. Joseph, MO) (KXA mix) and surgically prepared for intravital imaging of the brain as described [21,247,248]. CBA/CaJ mice were infected with PbA and subjected to brain IVM 1) on day 5 prior to the appearance of neurological signs, 2) on day 6–8 upon ECM development, or 3) on day 9 after the window of ECM development had passed. PyXL-infected mice were imaged upon the parasitemia exceeding 50% on day 5. Uninfected mice were used as controls. Prior to imaging, mice were inoculated with Evans blue and matching combinations of fluorescent markers. Despite severe illness of the animals, optimization of anesthesia, craniotomy, and injection of fluorescent markers allowed us to obtain good recordings from approximately 70% of the mice with ECM and 50% of the mice with hyperparasitemia.

Monitoring cell density and dynamics in the cortical microvasculature

iRBC were identified by fluorescent protein expression in the parasites or reflection of hemozoin [21]. The vascular lumen was visualized by intravenous injection of 100 µl of a 1% solution of Evans blue. Vascular endothelia were labeled intravenously with Alexa 488 or eFluor 450-conjugated rat anti-mouse PECAM-1 (CD31; clone MEC13.3, BioLegend, San Diego, CA) and phycoerythrin (PE)- or Alexa 647-conjugated rat anti-mouse

CD14 (clone Sa2-8, eBioscience). CD8+ T cells, CD4+ T cells, monocytes, macrophages, neutrophils, or platelets were labeled by intravenous injection of 3–5 µg of the following fluorochrome-conjugated monoclonal antibodies using appropriate color-matching combinations: PE-conjugated rat anti-mouse CD8a (clone 53-6.7; eBioscience, San Diego, CA), eFluor 450 or PE-conjugated rat anti-mouse CD4+ (clone GK 1.5, eBioscience), Pacific blue-conjugated rat anti-mouse CD11b (clone M1/70, BioLegend), eFluor 450-, PE- or Alexa 647-conjugated rat anti-mouse GR-1 (Ly-6G/6c; clone RB6-8C5, eBioscience and BioLegend), and eFluor 450-conjugated rat anti-mouse CD41 (clone MWReg30, eBioscience), respectively. ICAM-1 expression was visualized with intravenously inoculated PE-conjugated rat anti-mouse CD54 (clone YN 1/1.7.4, Biolegend). P-selectin was detected with PE-conjugated rat anti-human/mouse CD62p (KO2.3, eBioscience).

Quantification of leukocyte arrest and ICAM-1 expression

Multiple time sequences and 3D stacks were recorded for quantification of the number of arrested leukocytes in the vascular lumen. Depending on the experimental conditions, 20–45 postcapillary venules and arterioles were analyzed per mouse. Arrested leukocytes were defined in each vessel segment as cells that did not detach from the endothelial lining within the observation period. CD8+ T cells, CD4+ T cells, neutrophils, monocytes, and macrophages were quantified by counting the number of cells per square millimeter of vessel surface [249]. The relative density of the various leukocyte populations was determined in multiple fields of view per experimental condition and expressed as the mean ± SEM of arrested cells as well as the percentage of the total cell number. Velocities were measured with Imaris Track as described [250].

To quantify endothelial ICAM-1 expression, confocal 3D stacks of postcapillary venules or similarly sized arterioles were acquired from 2 mice each infected with PbA, PyXL, or no parasites. The fluorescence signal intensity across 10 (PbA) or 12 (PyXL and control) vessel volumes was collected from 3D data and quantified in ImageJ. To quantify leukocyte ICAM-1 expression, the relative fluorescence emission from individual leukocytes was measured from mice infected with PbA or PyXL. As for endothelial ICAM-1 expression, confocal 3D stacks were collected and projections were created in AutoDeblur. A total of 6 stacks from 2 mice per experimental condition were analyzed.

Brain leukocyte harvesting and flow cytometry

Leukocytes were prepared from the brain (cerebrum and cerebellum) using established procedures [251–253]. Briefly, mice were perfused intracardially with Mg^{2+} and Ca^{2+}-free PBS to dislodge nonadherent leukocytes. Next, the brain was removed and gently minced through a mesh strainer (mesh size: 100 µm; Fisher Scientific) using a syringe plunger. The homogenate was suspended in 10 ml HBSS containing 0.05% collagenase D (Roche Diagnostics, Indianapolis, IN), 0.1 µg/ml of the trypsin inhibitor TLCK (Sigma), 10 µg/ml DNase I (Sigma), and 10 mM Hepes buffer, pH 7.4. The tissue slurry was gently rocked at RT for 60 min and then allowed to settle at 1 g for 30 min. The supernatant was collected and 5 ml of the suspension was layered onto 10 ml of a density separation medium containing 7.5 ml of RPMI medium containing 10% FBS, 10 mM HEPES, and 2.5 ml Ficoll Paque (GE HealthCare) in a 50 ml conical centrifuge tube and centrifuged at 400 g for 30 min. The overlying media and tissue debris were removed, the entire gradient medium was diluted ten-fold with HBSS and centrifuged at 300 g for 10 min. Isolated leukocytes were washed twice with Mg^{2+} and Ca^{2+}-free PBS before phenotyping. A total of 10 PbA-infected mice with

ECM, 6 PbA-infected/FTY720-treated, and 6 PyXL-infected mice with hyperparasitemia were subjected to flow cytometric analysis. Uninfected control mice were not included in the analysis, because the cerebral microvasculature of these animals does not exhibit arrested leukocytes.

The following antibodies were used for leukocyte phenotyping: Total leukocytes were detected with PE-Cy7-conjugated rat anti-mouse CD45 (clone 30-F11; eBioscience, San Diego, CA), T cells with APC-Cy7-conjugated Armenian hamster anti-mouse CD3 (clone 145-2C11; BD Biosciences, San Jose, CA), CD8+ T cells with eFluor 450 or Alexa 700-conjugated rat anti-mouse CD8a (clone 53-6.7; eBioscience or Biolegend, San Diego, CA), CD4+ T cells with PE- Texas Red-conjugated rat anti-mouse CD4+ (clone RM4-5; Life Technologies, Carlsbad, CA, neutrophils with FITC-conjugated rat anti-mouse Ly6G (clone 1A8; Biolegend), monocytes with Alexa 700-conjugated rat anti-mouse Ly6C (clone HK 1.4; Biolegend), and macrophages with anti-mouse CD11b (clone M1/70; eBioscience) or PE- or eFluor 450-conjugated anti-mouse F4/80 (clone BM8; eBioscience). CCR5 (CD195) was detected with PE-conjugated rat anti-mouse CD195 (clone HM-CCR5; Biolegend), CD69 with Pacific Blue-conjugated rat anti-mouse CD69 (clone H1.2F3; Biolegend), ICAM-1 with APC-conjugated rat anti-mouse CD54 (clone YN1/1.7.4; eBioscience), and granzyme B with FITC-conjugated anti-mouse granzyme B (clone GB11; Biolegend). Data were acquired with a 5-laser, 17-color LSR II Analytic Flow Cytometer (BD Biosciences, San Jose, CA) and analyzed with FlowJo software (Treestar, Ashland, OR).

Microrheology

Time series showing the blood flow in postcapillary venules or similarly sized arterioles were acquired from mice infected with PbA, PyXL, or no parasites and converted to minimal projections to visualize the portion of the vascular lumen used for blood flow. The vascular lumen was visualized by IV inoculation of Evans blue [21]. IVM movies were converted to minimal projections to visualize the perfused center of the vessel. Multiple measurements were taken for each vessel to determine the entire vascular diameter (distance between endothelia) versus the perfused part of the vessel (dark center) (**Figures 1 and S2**). Vascular restriction is expressed as percent reduction in vessel diameter or cross-section.

Intravital confocal microscopy and image processing

The cortical microvasculature was imaged with an inverted Leica TCS SP2 AOBS confocal system as described [21]. Time series and 3D data sets were acquired with Leica Confocal Software [248,250,254]. Imaris 7.4 (Bitplane, Saint Paul, MN), Image-Pro Plus (Media Cybernetics, Bethesda, MD), AutoDeBlur (Media Cybernetics, Bethesda, MD), and NIH ImageJ were used for further image analysis, deconvolution, and 3D reconstruction.

Endothelial junction integrity

Blood was removed by perfusion with PBS via the left ventricle [251]. Brains were snap-frozen for preparation of cryostat sections. To determine the expression level of tight junction proteins, sections were fixed in 95% ice-cold ethanol for 30 minutes and then permeabilized in acetone for 1 min at RT. After blocking in 50% goat serum for 45 min, sections were labeled with rabbit polyclonal antibody against claudin 5 (34-1600), rabbit polyclonal anti-occludin (40-4700), mouse monoclonal anti-ZO1 (33-9100), all from Invitrogen. Rat monoclonal antibody anti-CD31 (553370) was from BD Biosciences. Sections were then incubated for 2 h at RT with secondary Alexa antibodies (Life Technologies) and mounted in Vectashield with DAPI (H1200, Vector Labs, Burlingame, CA). Depending on the experimental condition, 9–

16 images from various regions of the cerebrum and cerebellum were analyzed. Data were acquired at the same magnification with Zeiss Axiovison software using an Axio Imager-D2 Zeiss fluorescent microscope and imported into Image J for quantification of vascular leakage and tight junction protein expression. For tight junction protein expression, the fluorescence threshold was set with the "triangle" setting of Image J to limit the measurement of the brightest signal only, corresponding to the tight junctions. Ratios were then calculated by comparing the experimental groups with the control group using Excel. Significance was determined by t-test.

Statistical analysis

Statistical analysis was performed using Minitab® 17 (Minitab, State College, PA). Data sets were tested for normality and equal variances and when necessary data was Log10 transformed to obtain a normal distribution. Data were analyzed either by t-test, one-way ANOVA, or General Linear Model as appropriate. Where transformation was not successful, the non-parametric Mann-Whitney U test was used.

Supporting Information

Figure S1 Confocal intravital microscopy of the cortical microvasculature. Intravital microscopy of a PbA-infected CX3CR1$^{GFP/+}$ mouse with ECM shows that the postcapillary venules, capillaries, and arterioles analyzed in this study are embedded in green fluorescent microglia (arrows) and thus located in the cerebral cortex, i.e. below the layer of pial microvessels. Evans blue (red) visualizes the microvascular lumen, while blood cells are negatively stained (black). Leukocytes crawl slowly (large black circles), while RBCs move at bloodstream velocity and appear as dark streaks. Note that the vascular marker has leaked into the perivascular space. Scale bar = 50 μm.
(TIF)

Figure S2 Visualization of the luminal restriction of postcapillary venules during ECM. Examples of intravital movies and minimal projections of postcapillary venules from PbA-infected mice with ECM. **A, C**) Individual frames show postcapillary venules containing blood cells (dark circles or streaks) that are distorted due to the relatively slow confocal scan speed compared to the much faster blood flow. **B, D**) Minimal projections of the movies reveal that the functional vessel diameter (short arrows), i.e. the perfused portion of the vessel, is considerably reduced compared to the entire vessel diameter (long arrows). Visualization of the vascular lumen with Evans blue reveals a red zone along the endothelium of postcapillary venules that is devoid of RBC (dark). Scale bars = 20 μm. See **Video S1 and 2** for the corresponding dynamic data.
(TIF)

Figure S3 CD8+ T cell velocity during ECM and hyperparasitemia. CBA/CaJ mice infected with PbA or PyXL were inoculated with PE or eFluor 450-conjugated anti-CD8+a at the time of ECM or hyperparasitemia, respectively, and velocity and density of CD8+ T cells was determined by off-line analysis of intravital microscopy time sequences and 3D stacks, respectively. Mean velocity of intravascular CD8+ T cells during ECM (PbA) and hyperparasitemia (PyXL). The data represent the mean ± SEM of 61 cells from 5 PbA-infected and 10 cells from 5 PyXL-infected mice. Significance was calculated with 1-way ANOVA.
(TIF)

Figure S4 ICAM-1, CD69, and GrB expression in CD8+ T cells. Leukocytes were isolated from the brains of PbA-infected,

PbA-infected/FTY720-treated, and PyXL-infected mice. **A**) Flow cytometry reveals that FTY720 treatment reduces the ECM-associated accumulation of ICAM-1+ CD69+ GrB+ CD45^{hi} CD8+ T cells in the brain of PbA-infected mice to levels similar to those found in PyXL-infected mice with hyperparasitemia. The data are based on groups of at least 3 mice per experimental condition. Significance was determined with 1-way ANOVA followed by Tukey's test for multiple comparisons. See **Table S12** for details. **B–D**) Flow cytometry revealed no significant difference in the median expression levels of ICAM-1 (CD54) (**B**), CD69 (**C**), or GrB (**D**) in the CD45^{hi} subset of CD8+ T cells compared to PyXL-infected or PbA-infected/FTY720-treated mice. Data are based on 3 mice per group. Significance (*, $P<0.05$) was determined with 1-way ANOVA followed by Tukey's test for multiple comparisons.
(TIF)

Figure S5   Effect of FTY720 on endothelial CD14 expression. Postcapillary venule endothelia of PbA-infected mice are positive for CD14 at the time of ECM (green outline) (**A**). FTY720 treatment does not prevent endothelial CD14 expression in postcapillary venules (green outline) (**B**). PyXL-infected mice do not exhibit endothelial CD14 at the time of hyperparasitemia (**C**). Mice were inoculated with Evans blue (red) to visualize the vascular lumen and PE-conjugated anti-CD14. Note that monocytes (green open circles) are also CD14 positive (arrows in A and C). See **Videos S12, S13, and S16** for the corresponding dynamic data.
(TIF)

Figure S6   TJ protein expression in the cerebral cortex. Cryostat sections of the brains of PbA-infected CBA/CaJ mice with ECM (day 6–8; N = 4), PbA-infected and FTY720-treated mice that did not exhibit any neurological signs (day 8 or 9; N = 3), and PyXL-infected mice with hyperparasitemia (day 5; N = 3) were immunolabeled with specific antibodies the TJ proteins claudin-5, occludin, and ZO-1. Multiple confocal microscopy images per experimental condition were acquired and the overall TJ protein-specific fluorescence emission was quantified with ImageJ. No significant reduction in TJ protein expression was detected under the different infection and treatment conditions compared to uninfected control mice (N = 3).
(TIF)

Figure S7 TJ protein expression in the cerebellum. Cryostat sections of the brains of PbA-infected CBA/CaJ mice with ECM (day 6–8; N = 4), PbA-infected and FTY720-treated mice that did not exhibit any neurological signs (day 8 or 9; N = 3), and PyXL-infected mice with hyperparasitemia (day 5; N = 3) were immunolabeled with specific antibodies the TJ proteins claudin-5, occludin, and ZO-1. Multiple confocal microscopy images per experimental condition were acquired and the overall TJ protein-specific fluorescence emission of the microvascular endothelium quantified with ImageJ. No significant reduction in TJ protein expression was detected under the different infection and treatment conditions compared to uninfected control mice (N = 3).
(TIF)

Table S1   Number of mice examined by IVM. CBA/CaJ mice were infected with PbA, PyXL, or no parasites, and subjected to craniotomy, and surgically prepared for IVM. PbA infected mice were analyzed at the time of ECM (day 6–8), before the appearance of neurological signs (day 5), or after the window of ECM development had passed (day 9). PyXL infected mice were examined at the parasitemia exceeding 50%. Other mice were

treated daily with FTY720 starting one day before infection with PbA and examined by IVM on day 8 or 9.
(DOCX)

Table S2   CD8+ T cell density in PCV. CBA/CaJ mice were infected with PbA, PyXL, or no parasites, and subjected to craniotomy, and prepared for IVM. PbA infected mice were analyzed at the time of ECM (day 6–8), before the appearance of neurological signs (day 5), or after the window of ECM development had passed (day 9). PyXL infected mice were examined at the parasitemia exceeding 50%. CD8+ T cells were labeled by intravenous inoculation of PE-conjugated anti-CD8a. Significantly larger numbers of CD8+ T cells were recruited to PCV from mice with ECM compared to HP (* = p<0.05). No CD8+ T cells were found in the cortical microvasculature of PbA infected mice on day 5, in PbA infected mice that survived the critical period of ECM development without exhibiting neurological signs (day 9), or in uninfected control mice. The data represent the mean cell density/mm^2 ± SEM. The significance (PbA vs. PyXL) was determined by 1-way ANOVA. See also **Figures 2 and 3** and **Videos S6 and S7**.
(DOCX)

Table S3   CD4+ T cell density in PCV. CBA/CaJ mice were infected with PbA, PyXL, or no parasites, and subjected to craniotomy, and prepared for IVM. PbA infected mice were analyzed at the time of ECM (day 6–8), before the appearance of neurological signs (day 5), or after the window of ECM development had passed (day 9). PyXL infected mice were examined at the parasitemia exceeding 50%. Depending on the fluorescence of the parasites, CD8+ T cells were labeled by intravenous inoculation of PE- or eFluor 450-or PE-conjugated anti-CD4. Significantly larger numbers of CD4+ T cells were recruited to PCV from mice with ECM compared to HP (* = p< 0.05). No CD4+ T cells were found in the cortical microvasculature of PbA infected mice on day 5, in PbA infected mice that survived the critical period of ECM development without exhibiting neurological signs (day 9), or in uninfected control mice. The data represent the mean cell density/mm^2 ± STD. The significance (PbA vs. PyXL) was determined by 1-way ANOVA. See also **Figures 2 and 3** and **Videos S8 and S9**.
(DOCX)

Table S4   Neutrophil density in PCV. CBA/CaJ mice were infected with PbA, PyXL, or no parasites, and subjected to craniotomy, and prepared for IVM. PbA infected mice were analyzed at the time of ECM (day 6–8), before the appearance of neurological signs (day 5), or after the window of ECM development had passed (day 9). PyXL infected mice were examined at the parasitemia exceeding 50%. CD8+ T cells were labeled by intravenous inoculation of eFluor 450-conjugated GR-1. Significantly larger numbers of neutrophils were recruited to PCV from mice with ECM compared to HP (* = p<0.05). No neutrophils were found in the cortical microvasculature of PbA infected mice on day 5, in PbA infected mice that survived the critical period of ECM development without exhibiting neurological signs (day 9), or in uninfected control mice. The data represent the mean cell density/mm^2 ± SEM. The significance (PbA vs. PyXL) was determined by 1-way ANOVA. See also **Figures 2 and 3** and **Videos S10 and S11**.
(DOCX)

Table S5   Monocyte density in PCV. CBA/CaJ mice were infected with PbA, PyXL, or no parasites, and subjected to craniotomy, and prepared for IVM. PbA infected mice were analyzed at the time of ECM (day 6–8), before the appearance of

neurological signs (day 5), or after the window of ECM development had passed (day 9). PyXL infected mice were examined at the parasitemia exceeding 50%. CD8+ T cells were labeled by intravenous inoculation of PE-conjugated anti-CD14. Significantly larger numbers of monocytes were recruited to PCV from mice with ECM compared to HP (* = p<0.05). No monocytes were found in the cortical microvasculature of PbA infected mice on day 5, in PbA infected mice that survived the critical period of ECM development without exhibiting neurological signs (day 9), or in uninfected control mice. The data represent the mean cell density/mm^2 ± SEM. The significance (PbA vs. PyXL) was determined by 1-way ANOVA. See also **Figures 2 and 3** and **Videos S12 and S13**.
(DOCX)

Table S6 Macrophage density in PCV. CBA/CaJ mice were infected with PbA, PyXL, or no parasites, and subjected to craniotomy, and prepared for IVM. PbA infected mice were analyzed at the time of ECM (day 6–8), before the appearance of neurological signs (day 5), or after the window of ECM development had passed (day 9). PyXL infected mice were examined at the parasitemia exceeding 50%. CD8+ T cells were labeled by intravenous inoculation of eFluor 450-conjugated anti-CD11b. Significantly larger numbers of macrophages were recruited to PCV from mice with ECM compared to HP (* = p<0.05). No macrophages were found in the cortical microvasculature of PbA infected mice on day 5, in PbA infected mice that survived the critical period of ECM development without exhibiting neurological signs (day 9), or in uninfected control mice. The data represent the mean cell density/mm^2 ± SEM. The significance (PbA vs. PyXL) was determined by 1-way ANOVA. See also **Figures 2 and 3** and **Videos S14 and S15**.
(DOCX)

Table S7 Leukocyte accumulation in the brain. PbA-infected mice with ECM (day 6–8; N = 3), PbA-infected/FTY720-treated mice without neurological signs (day 8 or 9; N = 3), and PyXL-infected mice with HP (N = 3) were vascularly perfused prior to isolation of leukocytes from the cerebrum and cerebellum. Adherent cells were isolated and subjected to flow cytometry. CD45+ F4/80+ cells represent the entire macrophage population of the brain, while the CD45^{hi} F4/80+ macrophages are predominantly blood-derived. The data represent the average cell number per 50,000 events ± STD. Statistical analysis was performed using a 1-way ANOVA followed by Tukey's test for multiple comparisons. See also **Figure 3**.
(DOCX)

Table S8 CD45^{hi} and CD45^{lo} leukocyte subsets. PbA-infected mice with ECM (day 6–8; N = 3), PbA-infected/FTY720-treated mice without neurological signs (day 8 or 9; N = 3), and PyXL-infected mice with HP (day 5: N = 3) were vascularly perfused prior to isolation of leukocytes from the cerebrum and cerebellum. Adherent cells were isolated and subjected to flow cytometry. The data represent the average cell number per 50,000 events ± STD. Statistical analysis was performed using a 1-way ANOVA followed by Tukey's test for multiple comparisons. See also **Figure 4**.
(DOCX)

Table S9 ICAM-1 positive CD45^{hi} and CD45^{lo} leukocyte subsets. PbA-infected mice with ECM (day 6–8; N = 5), PbA-infected/FTY720-treated mice without neurological signs (day 8 or 9; N = 3), and PyXL-infected mice with HP (day 5: N = 3) were vascularly perfused prior to isolation of leukocytes from the cerebrum and cerebellum. Adherent cells were isolated and

subjected to flow cytometry. The data represent the average cell number per 50,000 events ± STD. Statistical analysis was performed using a 1-way ANOVA followed by Tukey's test for multiple comparisons. See also **Figure 4**.
(DOCX)

Table S10 CD69-positive CD45^{hi} and CD45^{lo} leukocyte subsets. PbA-infected mice with ECM (day 6–8; N = 3), PbA-infected/FTY720-treated mice without neurological signs (day 8 or 9; N = 3), and PyXL-infected mice with HP (day 5: N = 3) were vascularly perfused prior to isolation of leukocytes from the cerebrum and cerebellum. Adherent cells were isolated and subjected to flow cytometry. The data represent the average cell number per 50,000 events ± STD. Statistical analysis was performed using a 1-way ANOVA followed by Tukey's test for multiple comparisons. See also **Figure 4**.
(DOCX)

Table S11 GrB-positive CD45^{hi} and CD45^{lo} leukocyte subsets. PbA-infected mice with ECM (day 6–8; N = 3), PbA-infected/FTY720-treated mice without neurological signs (day 8 or 9; N = 3), and PyXL-infected mice with HP (day 5: N = 3) were vascularly perfused prior to isolation of leukocytes from the cerebrum and cerebellum. Adherent cells were isolated and subjected to flow cytometry. The data represent the average cell number per 50,000 events ± STD. Statistical analysis was performed using a 1-way ANOVA followed by Tukey's test for multiple comparisons. See also **Figure 4**.
(DOCX)

Table S12 Phenotype of CD45^{hi} CD8+ T cells. PbA-infected mice with ECM (day 6–8; N = 3), PbA-infected/FTY720-treated mice without neurological signs (day 8 or 9; N = 3), and PyXL-infected mice with HP (day 5: N = 3) were vascularly perfused prior to isolation of leukocytes from the cerebrum and cerebellum. Adherent cells were isolated and subjected to flow cytometry. The data represent the average cell number per 50,000 events ± STD. Statistical analysis was performed using a 1-way ANOVA followed by Tukey's test for multiple comparisons. See also **Figure S4**.
(DOCX)

Table S13 Endothelial ICAM-1 expression in the cortical microvasculature. Two PbA-infected mice with ECM (day 6–8), 2 PyXL-infected mice with HP (day 5), and 2 uninfected control mice were intravenously inoculated with PE-conjugated rat anti-mouse CD54 and subjected to IVM. Relative fluorescence emission was quantified as described in Materials & Methods and expressed as average ± STD. Statistical analysis was performed using 1-way ANOVA followed by Tukey's test for multiple comparisons. See also **Figure 5**.
(DOCX)

Table S14 Number of ICAM-1+ F4/80+ macrophages. PbA-infected mice with ECM (day 6–8; N = 3), PbA-infected/FTY720-treated mice without neurological signs (day 8 or 9; N = 3), and PyXL-infected mice with HP (day 5: N = 3) were vascularly perfused prior to isolation of leukocytes from the cerebrum and cerebellum. Adherent cells were isolated and subjected to flow cytometry. The data represent the average cell number per 50,000 events ± STD. T-test was used to determine significances. See also **Figure 6A and 6B**.
(DOCX)

Table S15 ICAM-1 expression level on F4/80+ macrophages. PbA-infected mice with ECM (day 6–8; N = 3), PbA-infected/FTY720-treated mice without neurological signs (day 8

or 9; N = 3), and PyXL-infected mice with HP (day 5: N = 3) were vascularly perfused prior to isolation of leukocytes from the cerebrum and cerebellum. Adherent cells were isolated and subjected to flow cytometry. The data represent the median cell number per 50,000 events ± STD. Statistical analysis was performed using a 1-way ANOVA followed by Tukey's Test for multiple comparisons. See also **Figure 6C**.
(DOCX)

Table S16 Tight junction protein expression in the cerebral cortex and cerebellum. Cryostat sections of brain tissue from PbA-infected CBA/CaJ mice with ECM (day 6–8; N = 4), PbA-infected and FTY720-treated mice that did not exhibit any neurological signs (day 8 or 9; N = 3), and PyXL-infected mice with HP (day 5; N = 3) were immunolabeled with specific antibodies the TJ proteins claudin-5, occludin, and ZO-1. Confocal microscopy images (3–4 per experimental condition) were acquired under identical conditions. Images were imported into ImageJ for quantification of the average TJ protein-specific fluorescence emission with the threshold set to Triangle. The data represent average fluorescence intensity ± SD in the entire field of observation. Significant differences (* = $P < 0.05$) in TJ protein expression under the different infection and treatment conditions were determined by t-test in relation to uninfected control mice (N = 3). See also **Figure S6 and S7**.
(DOCX)

Video S1 ECM is associated with a significant reduction in the venous blood flow. Intravital microscopy of a PbA-infected CBA/CaJ mouse injected with Evans blue (red) upon development of ECM symptoms. Arrested or crawling leukocytes (dark circles) prevent access to the endothelium so that the marginal zone of the postcapillary venule lumen lacks blood cells traveling in the bloodstream (dark streaks). Note the extensive leakage of Evans blue from the cortical postcapillary venules in the surrounding tissue. Scale bar = 20 µm.
(AVI)

Video S2 ECM is associated with a significant reduction in the venous blood flow. Intravital microscopy of a PbA-infected CBA/CaJ mouse injected with Evans blue (red) upon development of ECM symptoms. Arrested leukocytes (dark circles) prevent access to the endothelium so that the marginal zone of the postcapillary venule lumen lacks blood cells traveling in the bloodstream (dark streaks). Evans blue has leaked from the cortical postcapillary venules in the surrounding tissue. Scale bar = 20 µm.
(AVI)

Video S3 The arteriolar microrheology remains unaltered during ECM. Intravital microscopy of a PbA-infected CBA/CaJ mouse showing normal blood flow in a cortical arteriole (vessel running horizontally). Note that the entire microvascular lumen is used for the blood flow. The vascular lumen is visualized with Evans blue (red), while blood cells are negatively stained (dark streaks). Scale bar = 20 µm.
(AVI)

Video S4 The venous microrheology remains unaltered during hyperparasitemia. Intravital microscopy of a PyXL infected CBA/CaJ mouse exhibiting normal blood flow in a cortical postcapillary venules. Note that the entire microvascular lumen is used for the blood flow. The vascular lumen is visualized with Evans blue (red), while blood cells are negatively stained (dark streaks). Scale bar = 20 µm.
(AVI)

Video S5 Normal venous microrheology of uninfected control mice. Intravital microscopy of an uninfected control CBA/CaJ mouse exhibiting normal blood flow in a cortical postcapillary venule. Note that the entire microvascular lumen is used for the blood flow. The vascular lumen is visualized with Evans blue (red), while blood cells are negatively stained (dark streaks). Scale bar = 20 µm.
(AVI)

Video S6 CD8+ T cell behavior during ECM. Intravital microscopy of a PbA infected CBA/CaJ mouse with ECM showing a large number of CD8+ T cells (green surface label) crawling along the endothelium of a cortical postcapillary venules with a typical leading edge and trailing uropod (arrow). CD8+ T cells were surface-labeled by intravenous inoculation of PE-conjugated anti-CD8a. The vascular lumen was visualized with Evans blue (red). Scale bar = 20 µm.
(AVI)

Video S7 CD8+ T cell behavior during hyperparasitemia. Intravital microscopy of a PyXL infected CBA/CaJ mouse with hyperparasitemia showing a small number of CD8+ T cells (green surface label) crawling along the endothelium of a cortical postcapillary venules. CD8+ T cells were labeled by intravenous inoculation of eFluor 450-conjugated anti-CD8a (false-colored in green). The vascular lumen was visualized with Evans blue (red). Scale bar = 20 µm.
(AVI)

Video S8 CD4+ T cell behavior during ECM. Intravital microscopy of a PbA infected CBA/CaJ mouse with ECM showing CD4+ T cells (green surface label) arrested on the endothelium of a cortical postcapillary venules. CD4+ T cells were labeled by intravenous inoculation of PE-conjugated anti-CD4+. The vascular lumen was visualized with Evans blue (red). The numerous large leukocytes (dark circles) represent most likely monocytes and macrophages. Scale bar = 20 µm.
(AVI)

Video S9 CD4+ T cell behavior during hyperparasitemia. Intravital microscopy of a PyXL infected CBA/CaJ mouse with hyperparasitemia showing CD4+ T cells (green surface label) arrested on the endothelium of a cortical postcapillary venules. CD4+ T cells were labeled by intravenous inoculation of PE-conjugated anti-CD4+. The vascular lumen was visualized with Evans blue (red). Scale bar = 20 µm.
(AVI)

Video S10 Neutrophil behavior during ECM. Intravital microscopy of a PbA infected CBA/CaJ mouse with ECM showing large numbers of neutrophils (green surface label) arrested on the endothelium of a cortical postcapillary venules. Neutrophils were labeled by intravenous inoculation of eFluor 450-conjugated GR-1 (false-colored in green). The vascular lumen was visualized with Evans blue (red). Scale bar = 20 µm.
(AVI)

Video S11 Neutrophil behavior during hyperparasitemia. Intravital microscopy of a PyXL infected CBA/CaJ mouse with hyperparasitemia showing a small number of neutrophils (green surface label) arrested on the endothelium of a cortical postcapillary venules. Neutrophils were labeled by intravenous inoculation of eFluor 450-conjugated GR-1 (false-colored in green). The vascular lumen was visualized with Evans blue (red). Scale bar = 20 µm.
(AVI)

Video S12 Monocyte behavior during ECM. Intravital microscopy of a PbA infected CBA/CaJ mouse with ECM showing monocytes (green surface label) arrested on the endothelium of a cortical postcapillary venules. Monocytes were labeled by intravenous inoculation of PE-conjugated anti-CD14. Note that the fluorescent marker also labels the endothelium of the postcapillary venules. The vascular lumen was visualized with Evans blue (red). The numerous large leukocytes (dark circles) represent most likely monocytes and macrophages. Scale bar = 20 μm.
(AVI)

Video S13 Monocyte behavior during hyperparasitemia. Intravital microscopy of a PyXL infected CBA/CaJ mouse with hyperparasitemia showing a monocyte (green) arrested on the endothelium of a cortical postcapillary venules. The mouse was intravenously inoculated with PE-conjugated anti-CD14. Note that CD14 is not expressed on the endothelium of the postcapillary venules during hyperparasitemia. The vascular lumen was visualized with Evans blue (red). Scale bar = 20 μm.
(AVI)

Video S14 Macrophage behavior during ECM. Intravital microscopy of a PbA infected CBA/CaJ mouse with ECM showing macrophages (green surface label) arrested on the endothelium of a cortical postcapillary venules. Macrophages were labeled by intravenous inoculation of Pacific blue-conjugated anti-CD11b. The vascular lumen was visualized with Evans blue (red). Scale bar = 20 μm.
(AVI)

Video S15 Macrophage behavior during hyperparasitemia. Intravital microscopy of a PyXL infected CBA/CaJ mouse with hyperparasitemia showing macrophages (green surface label) arrested on the endothelium of a cortical postcapillary venules. Macrophages were labeled by intravenous inoculation of Pacific blue-conjugated anti-CD11b (false-colored in green). The vascular lumen was visualized with Evans blue (red). Scale bar = 20 μm.
(AVI)

Video S16 Monocyte behavior after FTY720 treatment. Intravital microscopy stack of a PbA infected and FTY720-treated CBA/CaJ mouse without ECM showing monocytes (green surface label) arrested on the endothelium of a cortical postcapillary venules. Monocytes were labeled by intravenous inoculation of PE-conjugated anti-CD14. The endothelium of the postcapillary venules is CD14-positive despite the FTY720 treatment. Note that the smaller arteriole on the left is CD14-negative. The vascular lumen was visualized with Evans blue (red). Scale bar = 20 μm.
(AVI)

Video S17 ICAM-1 is upregulated during ECM. Intravital microscopy stack showing that ICAM-1 (gray) is expressed on the surface of postcapillary venules and, to a lesser degree, also on arteriolar endothelia (day 6–8 after infection with PbA). Note that some arrested leukocytes also express ICAM-1 (gray surface label). Scale bar = 20 μm.
(AVI)

Video S18 ICAM-1 is upregulated during hyperparasitemia. Intravital microscopy stack showing that ICAM-1 (gray) is expressed on the surface of postcapillary venules and, to a lesser degree, also on arteriolar endothelia (day 5 after infection with PyXL). Note that the number of arrested ICAM-1 expressing leukocytes (gray surface label) is lower during hyperparasitemia compared to ECM (**Video S12**). Scale bar = 20 μm.
(AVI)

Video S19 ICAM-1 expression in an uninfected control mouse. Intravital microscopy stack showing a lower level of ICAM-1 (gray) expression on the surface of postcapillary venules compared to mice with ECM (**Video S12**) or hyperparasitemia (**Video S13**). ICAM-1 expressing leukocytes are absent. Scale bar = 20 μm.
(AVI)

Video S20 ECM is associated with platelet arrest and P-selectin expression. CBA/CaJ mouse infected with PbA and inoculated with eFluor 450-conjugated anti-CD41 at the time of ECM. The intravital microscopy movie shows small clusters of marginalized platelets (blue) whose surface is positive for PE-conjugated anti-CD62p (green). The lumen of the cortical postcapillary venules is visualized with Evans blue (red). Scale bar = 20 μm.
(AVI)

Video S21 Mice with ECM exhibit strings of platelets in postcapillary venules. At the time of ECM, a PbA-infected CBA/CaJ mouse that was inoculated with eFluor 450-conjugated anti-CD41 (blue). A postcapillary venule contains a string of platelets (blue), which appears to be attached to a cluster of marginalized platelets. Scale bar = 20 μm.
(AVI)

Video S22 Hyperparasitemia is not associated with platelet arrest or P-selectin expression. Intravital microscopy of a CBA/CaJ mouse infected with PyXL-RFP iRBC shows eFluor 450-labeled platelets (blue) circulating at blood velocity. There is no evidence for P-selectin labeling, although the mouse was inoculated with a PE-conjugated specific antibody (green). The lumen of the cortical PVC is visualized with Evans blue (red). Scale bar = 20 μm.
(AVI)

Author Contributions

Conceived and designed the experiments: AN AM FS UF. Performed the experiments: AN AM FS UF. Analyzed the data: AN AM FS UF. Contributed reagents/materials/analysis tools: PL RD UF. Wrote the paper: AN UF. Provided expertise in flow cytometry: NMG UMG.

References

1. WHO (2013) World Malaria Report: 2013. Geneva, Switzerland: World Health Organization.
2. Milner DA, Jr. (2010) Rethinking cerebral malaria pathology. Curr Op Infect Dis 23: 456–463.
3. Haldar K, Murphy SC, Milner DA, Taylor TE (2007) Malaria: mechanisms of erythrocytic infection and pathological correlates of severe disease. Annu Rev Pathol 2: 217–249.
4. Clark IA, Awburn MM, Whitten RO, Harper CG, Liomba NG, et al. (2003) Tissue distribution of migration inhibitory factor and inducible nitric oxide synthase in falciparum malaria and sepsis in African children. Malaria J 2: 6.
5. Hunt NH, Grau GE, Engwerda C, Barnum SR, van der Heyde H, et al. (2010) Murine cerebral malaria: the whole story. Trends Parasitol 26: 272–274.

6. de Souza JB, Hafalla JCR, Riley EM, Couper KN (2010) Cerebral malaria: why experimental murine models are required to understand the pathogenesis of disease. Parasitology 137: 755–772.

7. White VA, Lewallen S, Beare NA, Molyneux ME, Taylor TE (2009) Retinal pathology of pediatric cerebral malaria in Malawi. PLoS ONE 4: e4317.

8. Beare NA, Lewallen S, Taylor TE, Molyneux ME (2011) Redefining cerebral malaria by including malaria retinopathy. Future Microbiol 6: 349–355.

9. Lou J, Lucas R, Grau GE (2001) Pathogenesis of cerebral malaria: recent experimental data and possible applications for humans. Clin Microbiol Rev 14: 810–820.

10. Lamb TJ, Brown DE, Potocnik AJ, Langhorne J (2006) Insights into the immunopathogenesis of malaria using mouse models. Expert Rev Mol Med 8: 1–22.

11. Engwerda C, Belnoue E, Gruner AC, Renia L (2005) Experimental models of cerebral malaria. Curr Top Microbiol Immunol 297: 103–143.

12. Renia L, Potter SM, Mauduit M, Rosa DS, Kayibanda M, et al. (2006) Pathogenic T cells in cerebral malaria. Int J Parasitol 36: 547–554.

13. Combes V, Coltel N, Faille D, Wassmer SC, Grau GE (2006) Cerebral malaria: role of microparticles and platelets in alterations of the blood-brain barrier. Int J Parasitol 36: 541–546.

14. Grau GE, Piguet PF, Vassalli P, Lambert PH (1989) Tumor-necrosis factor and other cytokines in cerebral malaria: experimental and clinical data. Immunol Rev 112: 49–70.

15. Langhorne J, Quin SJ, Sanni LA (2002) Mouse models of blood-stage malaria infections: immune responses and cytokines involved in protection and pathology. Chem Immunol 80: 204–228.

16. Sanni LA (2001) The role of cerebral oedema in the pathogenesis of cerebral malaria. Redox Rep 6: 137–142.

17. Penet M-F, Viola A, Confort-Gouny S, Le Fur Y, Duhamel G, et al. (2005) Imaging experimental cerebral malaria in vivo: significant role of ischemic brain edema. J Neurosci 25: 7352–7358.

18. Cox D, McConkey S (2010) The role of platelets in the pathogenesis of cerebral malaria. Cell Mol Life Sci 67: 557–568.

19. Moxon CA, Heyderman RS, Wassmer SC (2009) Dysregulation of coagulation in cerebral malaria. Mol Biochem Parasitol 166: 99–108.

20. Combes V, Rosenkranz AR, Redard M, Pizzolato G, Lepidi H, et al. (2004) Pathogenic role of P-selectin in experimental cerebral malaria: importance of the endothelial compartment. Am J Pathol 164: 781–786.

21. Nacer A, Movila A, Baer K, Mikolajczak SA, Kappe SH, et al. (2012) Neuroimmunological blood brain barrier opening in experimental cerebral malaria. PLoS Pathog 8: e1002982.

22. Faille D, El-Assaad F, Alessi MC, Fusai T, Combes V, et al. (2009) Platelet-endothelial cell interactions in cerebral malaria: the end of a cordial understanding. Thromb Haemost 102: 1093–1102.

23. Faille D, Combes V, Mitchell AJ, Fontaine A, Juhan-Vague I, et al. (2009) Platelet microparticles: a new player in malaria parasite cytoadherence to human brain endothelium. FASEB J 23: 3449–3458.

24. Barbier M, Faille D, Loriod B, Textoris J, Camus C, et al. (2011) Platelets alter gene expression profile in human brain endothelial cells in an in vitro model of cerebral malaria. PLoS ONE 6: e19651.

25. Mfonkeu JB, Gouado I, Kuate HF, Zambou O, Combes V, et al. (2010) Biochemical markers of nutritional status and childhood malaria severity in Cameroon. Br J Nutr 104: 886–892.

26. Belnoue E, Kayibanda M, Vigario AM, Deschemin JC, van Rooijen N, et al. (2002) On the pathogenic role of brain-sequestered alphabeta CD8+ T cells in experimental cerebral malaria. J Immunol 169: 6369–6375.

27. Claser C, Malleret B, Gun SY, Wong AY, Chang ZW, et al. (2011) CD8 T cells and IFN-gamma mediate the time-dependent accumulation of infected red blood cells in deep organs during experimental cerebral malaria. PLoS ONE 6: e18720.

28. McQuillan JA, Mitchell AJ, Ho YF, Combes V, Ball HJ, et al. (2011) Coincident parasite and CD8 T cell sequestration is required for development of experimental cerebral malaria. Int J Parasitol 41: 155–163.

29. Hermsen C, van de Wiel T, Mommers E, Sauerwein R, Eling W (1997) Depletion of CD4+ or CD8+ T-cells prevents Plasmodium berghei induced cerebral malaria in end-stage disease. Parasitology 114 (Pt 1): 7–12.

30. Amante FH, Haque A, Stanley AC, Rivera Fde L, Randall LM, et al. (2010) Immune-mediated mechanisms of parasite tissue sequestration during experimental cerebral malaria. J Immunol 185: 3632–3642.

31. Franke-Fayard B, Janse CJ, Cunha-Rodrigues M, Ramesar J, Buscher P, et al. (2005) Murine malaria parasite sequestration: CD36 is the major receptor, but cerebral pathology is unlinked to sequestration. Proc Natl Acad Sci U S A 102: 11468–11473.

32. Haque A, Best SE, Unosson K, Amante FH, de Labastida F, et al. (2011) Granzyme B expression by CD8+ T cells is required for the development of experimental cerebral malaria. J Immunol 186: 6148–6156.

33. Nitcheu J, Bonduelle O, Combadiere C, Tefit M, Seilhean D, et al. (2003) Perforin-dependent brain-infiltrating cytotoxic CD8+ T lymphocytes mediate experimental cerebral malaria pathogenesis. J Immunol 170: 2221–2228.

34. Baptista FG, Pamplona A, Pena AC, Mota MM, Pied S, et al. (2010) Accumulation of Plasmodium berghei-infected red blood cells in the brain is crucial for the development of cerebral malaria in mice. Infect Immun 78: 4033–4039.

35. Amante FH, Haque A, Stanley AC, Rivera FdL, Randall LM, et al. (2010) Immune-mediated mechanisms of parasite tissue sequestration during experimental cerebral malaria. J Immunol 185: 3632–3642.

36. Pais TF, Chatterjee S (2005) Brain macrophage activation in murine cerebral malaria precedes accumulation of leukocytes and CD8+ T cell proliferation. J Neuroimmunol 163: 73–83.

37. Potter S, Chan-Ling T, Ball HJ, Mansour H, Mitchell A, et al. (2006) Perforin mediated apoptosis of cerebral microvascular endothelial cells during experimental cerebral malaria. Int J Parasitol 36: 485–496.

38. Owens T, Bechmann I, Engelhardt B (2008) Perivascular spaces and the two steps to neuroinflammation. J Neuropathol Exp Neurol 67: 1113–1121.

39. Finney CA, Hawkes CA, Kain DC, Dhabangi A, Musoke C, et al. (2011) S1P is associated with protection in human and experimental cerebral malaria. Mol Med 17: 717–725.

40. Kipp M, Amor S (2012) FTY720 on the way from the base camp to the summit of the mountain: relevance for remyelination. Mult Scler 18: 258–263.

41. Hla T, Brinkmann V (2011) Sphingosine 1-phosphate (S1P): Physiology and the effects of S1P receptor modulation. Neurology 76: S3–8.

42. Brinkmann V, Billich A, Baumruker T, Heining P, Schmouder R, et al. (2010) Fingolimod (FTY720): discovery and development of an oral drug to treat multiple sclerosis. Nat Rev Drug Discov 9: 883–897.

43. Metzler B, Gfeller P, Wieczorek G, Li J, Nuesslein-Hildesheim B, et al. (2008) Modulation of T cell homeostasis and alloreactivity under continuous FTY720 exposure. Int Immunol 20: 633–644.

44. Taylor PA, Ehrhardt MJ, Lees CJ, Tolar J, Weigel BJ, et al. (2007) Insights into the mechanism of FTY720 and compatibility with regulatory T cells for the inhibition of graft-versus-host disease (GVHD). Blood 110: 3480–3488.

45. Idzko M, Hammad H, van Nimwegen M, Kool M, Muller T, et al. (2006) Local application of FTY720 to the lung abrogates experimental asthma by altering dendritic cell function. J Clin Invest 116: 2935–2944.

46. Brinkmann V, Cyster JG, Hla T (2004) FTY720: sphingosine 1-phosphate receptor-1 in the control of lymphocyte egress and endothelial barrier function. Am J Transplant 4: 1019–1025.

47. Sanchez T, Estrada-Hernandez T, Paik JH, Wu MT, Venkataraman K, et al. (2003) Phosphorylation and action of the immunomodulator FTY720 inhibits vascular endothelial cell growth factor-induced vascular permeability. J Biol Chem 278: 47281–47290.

48. Lee MJ, Thangada S, Claffey KP, Ancellin N, Liu CH, et al. (1999) Vascular endothelial cell adherens junction assembly and morphogenesis induced by sphingosine-1-phosphate. Cell 99: 301–312.

49. Dev KK, Mullershausen F, Mattes H, Kuhn RR, Bilbe G, et al. (2008) Brain sphingosine-1-phosphate receptors: implication for FTY720 in the treatment of multiple sclerosis. Pharmacol Ther 117: 77–93.

50. Newton CR, Kirkham FJ, Winstanley PA, Pasvol G, Peshu N, et al. (1991) Intracranial pressure in African children with cerebral malaria. Lancet 337: 573–576.

51. Shih AY, Blinder P, Tsai PS, Friedman B, Stanley G, et al. (2013) The smallest stroke: occlusion of one penetrating vessel leads to infarction and a cognitive deficit. Nat Neurosci 16: 55–63.

52. Risser L, Plouraboue F, Steyer A, Cloetens P, Le Duc G, et al. (2007) From homogeneous to fractal normal and tumorous microvascular networks in the brain. J Cereb Blood Flow Metab 27: 293–303.

53. Medana IM, Turner GD (2006) Human cerebral malaria and the blood-brain barrier. Int J Parasitol 36: 555–568.

54. Kampondeni SD, Potchen MJ, Beare NA, Seydel KB, Glover SJ, et al. (2013) MRI findings in a cohort of brain injured survivors of pediatric cerebral malaria. Am J Trop Med Hyg 88: 542–546.

55. Seydel K, Kampondeni S, Potchen M, Birbeck G, Molyneux M, et al. (2011) Clinical Correlates of Magnetic Resonance Imaging in Pediatric Cerebral Malaria. ASTMH Annual Meeting Philadelphia, PA: American Society of Tropical Medicine and Hygiene.

56. Ford AL, Goodsall AL, Hickey WF, Sedgwick JD (1995) Normal adult ramified microglia separated from other central nervous system macrophages by flow cytometric sorting. Phenotypic differences defined and direct ex vivo antigen presentation to myelin basic protein-reactive CD4+ T cells compared. J Immunol 154: 4309–4321.

57. Dietrich JB (2002) The adhesion molecule ICAM-1 and its regulation in relation with the blood-brain barrier. J Neuroimmunol 128: 58–68.

58. Kim H, Higgins S, Liles WC, Kain KC (2011) Endothelial activation and dysregulation in malaria: a potential target for novel therapeutics. Curr Opin Hematol 18: 177–185.

59. Chakravorty SJ, Craig A (2005) The role of ICAM-1 in Plasmodium falciparum cytoadherence. Eur J Cell Biol 84: 15–27.

60. Sherman IW, Eda S, Winograd E (2003) Cytoadherence and sequestration in Plasmodium falciparum: defining the ties that bind. Microbes Infect/Institut Pasteur 5: 897–909.

61. Ho M, White NJ (1999) Molecular mechanisms of cytoadherence in malaria. Am J Physiol 276: C1231–1242.

62. Amani V, Vigario AM, Belnoue E, Marussig M, Fonseca L, et al. (2000) Involvement of IFN-gamma receptor-medicated signaling in pathology and anti-malarial immunity induced by Plasmodium berghei infection. Eur J Immunol 30: 1646–1655.

63. Kaul DK, Liu XD, Nagel RL, Shear HL (1998) Microvascular hemodynamics and in vivo evidence for the role of intercellular adhesion molecule-1 in the

sequestration of infected red blood cells in a mouse model of lethal malaria. Am J Trop Med Hyg 58: 240–247.

64. Shear HL, Marino MW, Wanidworanun C, Berman JW, Nagel RL (1998) Correlation of increased expression of intercellular adhesion molecule-1, but not high levels of tumor necrosis factor-alpha, with lethality of *Plasmodium yoelii* 17XL, a rodent model of cerebral malaria. Am J Trop Med Hyg 59: 852–858.

65. Haque A, Echchannaoui H, Seguin R, Schwartzman J, Kasper LH, et al. (2001) Cerebral malaria in mice: interleukin-2 treatment induces accumulation of gammadelta T cells in the brain and alters resistant mice to susceptible-like phenotype. Am J Pathol 158: 163–172.

66. Ramos TN, Bullard DC, Darley MM, McDonald K, Crawford DF, et al. (2013) Experimental cerebral malaria develops independently of endothelial expression of intercellular adhesion molecule-1 (icam-1). J Biol Chem 288: 10962–10966.

67. Goebeler M, Roth J, Kunz M, Sorg C (1993) Expression of intercellular adhesion molecule-1 by murine macrophages is up-regulated during differentiation and inflammatory activation. Immunobiology 188: 159–171.

68. Ruetten H, Thiemermann C, Perretti M (1999) Upregulation of ICAM-1 expression on J774.2 macrophages by endotoxin involves activation of NF-kappaB but not protein tyrosine kinase: comparison to induction of iNOS. Mediators Inflamm 8: 77–84.

69. Novosad J, Holicka M, Novosadova M, Krejsek J, Krcmova I (2011) Rapid onset of ICAM-1 expression is a marker of effective macrophages activation during infection of Francisella tularensis LVS in vitro. Folia Microbiol (Praha) 56: 149–154.

70. Fattal-German M, Le Roy Ladurie F, Lecerf F, Berrih-Aknin S (1996) Expression of ICAM-1 and TNF alpha in human alveolar macrophages from lung-transplant recipients. Ann N Y Acad Sci 796: 138–148.

71. Jenne CN, Kubes P (2013) Immune surveillance by the liver. Nat Immunol 14: 996–1006.

72. Ochoa CD, Wu S, Stevens T (2010) New developments in lung endothelial heterogeneity: Von Willebrand factor, P-selectin, and the Weibel-Palade body. Semin Thromb Hemost 36: 301–308.

73. Lowenstein CJ, Morrell CN, Yamakuchi M (2005) Regulation of Weibel-Palade body exocytosis. Trends Cardiovasc Med 15: 302–308.

74. Wassmer SC, Combes V, Candal FJ, Juhan-Vague I, Grau GE (2006) Platelets potentiate brain endothelial alterations induced by Plasmodium falciparum. Infection and Immunity 74: 645–653.

75. Wassmer SC, Lepolard C, Traore B, Pouvelle B, Gysin J, et al. (2004) Platelets reorient *Plasmodium falciparum*-infected erythrocyte cytoadhesion to activated endothelial cells. J Infect Dis 189: 180–189.

76. Grau GE, Mackenzie CD, Carr RA, Redard M, Pizzolato G, et al. (2003) Platelet accumulation in brain microvessels in fatal pediatric cerebral malaria. J Infect Dis 187: 461–466.

77. Linares M, Marin-Garcia P, Perez-Benavente S, Sanchez-Nogueiro J, Puyet A, et al. (2012) Brain-derived neurotrophic factor and the course of experimental cerebral malaria. Brain Res 1490: 210–224.

78. Zanini GM, Cabrales P, Barkho W, Frangos JA, Carvalho LJ (2011) Exogenous nitric oxide decreases brain vascular inflammation, leakage and venular resistance during Plasmodium berghei ANKA infection in mice. J Neuroinflammation 8: 66.

79. Bridges DJ, Bunn J, van Mourik JA, Grau G, Preston RJ, et al. (2010) Rapid activation of endothelial cells enables *Plasmodium falciparum* adhesion to platelet-decorated von Willebrand factor strings. Blood 115: 1472–1474.

80. Camerer E, Regard JB, Cornelissen I, Srinivasan Y, Duong DN, et al. (2009) Sphingosine-1-phosphate in the plasma compartment regulates basal and inflammation-induced vascular leak in mice. J Clin Invest 119: 1871–1879.

81. Oo ML, Chang SH, Thangada S, Wu MT, Rezaul K, et al. (2011) Engagement of S1P(1)-degradative mechanisms leads to vascular leak in mice. J Clin Invest 121: 2290–2300.

82. Frevert U, Nacer A (2013) Immunobiology of Plasmodium in liver and brain. Parasite Immunol 35: 267–282.

83. Pries AR, Secomb TW, Gaehtgens P (2000) The endothelial surface layer. Pflugers Arch 440: 653–666.

84. Reitsma S, Slaaf DW, Vink H, van Zandvoort MA, oude Egbrink MG (2007) The endothelial glycocalyx: composition, functions, and visualization. Pflugers Arch 454: 345–359.

85. Fels J, Jeggle P, Liashkovich I, Peters W, Oberleithner H (2014) Nanomechanics of vascular endothelium. Cell Tissue Res 355: 727–737.

86. Alphonsus CS, Rodseth RN (2014) The endothelial glycocalyx: a review of the vascular barrier. Anaesthesia 69: 777–784.

87. Berendt AR, Tumer GD, Newbold CI (1994) Cerebral malaria: the sequestration hypothesis. Parasitol Today 10: 412–414.

88. Clark IA, Rockett KA (1994) The cytokine theory of human cerebral malaria. Parasitol Today 10: 410–412.

89. Grau GE, de Kossodo S (1994) Cerebral malaria: mediators, mechanical obstruction or more? Parasitol Today 10: 408–409.

90. Cabrales P, Martins YC, Ong PK, Zanini GM, Frangos JA, et al. (2013) Cerebral tissue oxygenation impairment during experimental cerebral malaria. Virulence 4: 686–697.

91. Koutsiaris AG, Tachmitzi SV, Batis N, Kotoula MG, Karabatsas CH, et al. (2007) Volume flow and wall shear stress quantification in the human conjunctival capillaries and post-capillary venules in vivo. Biorheology 44: 375–386.

92. Ampawong S, Combes V, Hunt NH, Radford J, Chan-Ling T, et al. (2011) Quantitation of brain edema and localisation of aquaporin 4 expression in relation to susceptibility to experimental cerebral malaria. Int J Clin Exp Pathol 4: 566–574.

93. Mohanty S, Mishra SK, Patnaik R, Dutt AK, Pradhan S, et al. (2011) Brain swelling and mannitol therapy in adult cerebral malaria: a randomized trial. Clin Infect Dis 53: 349–355.

94. Looareesuwan S, Wilairatana P, Krishna S, Kendall B, Vannaphan S, et al. (1995) Magnetic resonance imaging of the brain in patients with cerebral malaria. Clin Infect Dis 21: 300–309.

95. Newton CR, Crawley J, Sowumni A, Waruiru C, Mwangi I, et al. (1997) Intracranial hypertension in Africans with cerebral malaria. Arch Dis Child 76: 219–226.

96. Waller D, Crawley J, Nosten F, Chapman D, Krishna S, et al. (1991) Intracranial pressure in childhood cerebral malaria. Trans R Soc Trop Med Hyg 85: 362–364.

97. Murphy S, Cserti-Gazdewich C, Dhabangi A, Musoke C, Nabukeera-Barungi N, et al. (2011) Ultrasound findings in *Plasmodium falciparum* malaria: a pilot study. Pediatr Crit Care Med 12: e58–63.

98. Newton CR, Marsh K, Peshu N, Kirkham FJ (1996) Perturbations of cerebral hemodynamics in Kenyans with cerebral malaria. Pediatr Neurol 15: 41–49.

99. Potchen MJ, Kampondeni SD, Seydel KB, Birbeck GL, Hammond CA, et al. (2012) Acute brain MRI findings in 120 Malawian children with cerebral malaria: new insights into an ancient disease. AJNR Am J Neuroradiol 33: 1740–1746.

100. Cabrales P, Zanini GM, Meays D, Frangos JA, Carvalho LJM (2010) Murine cerebral malaria is associated with a vasospasm-like microcirculatory dysfunction, and survival upon rescue treatment is markedly increased by nimodipine. Am J Pathol 176: 1306–1315.

101. Kennan RP, Machado FS, Lee SC, Desruisseaux MS, Wittner M, et al. (2005) Reduced cerebral blood flow and N-acetyl aspartate in a murine model of cerebral malaria. Parasitol Res 96: 302–307.

102. Martins YC, Daniel-Ribeiro CT (2013) A new hypothesis on the manifestation of cerebral malaria: The secret is in the liver. Med Hypotheses 81: 777–783.

103. Holtmaat A, Bonhoeffer T, Chow DK, Chuckowree J, De Paola V, et al. (2009) Long-term, high-resolution imaging in the mouse neocortex through a chronic cranial window. Nat Protocols 4: 1128–1144.

104. Mostany R, Portera-Cailliau C (2008) A craniotomy surgery procedure for chronic brain imaging. J Vis Exp: e680 610.3791/3680, DOI: 3710.3791/3680.

105. King-VanVlack CE, Mewburn JD, Chapler CK, MacDonald PH (2003) Hemodynamic and proinflammatory actions of endothelin-1 in guinea pig small intestine submucosal microcirculation. Am J Physiol Gastrointest Liver Physiol 284: G940–948.

106. Callera GE, Touyz RM, Teixeira SA, Muscara MN, Carvalho MH, et al. (2003) ETA receptor blockade decreases vascular superoxide generation in DOCA-salt hypertension. Hypertension 42: 811–817.

107. McCarron RM, Wang L, Stanimirovic DB, Spatz M (1993) Endothelin induction of adhesion molecule expression on human brain microvascular endothelial cells. Neurosci Lett 156: 31–34.

108. Freeman BD, Machado FS, Tanowitz HB, Desruisseaux MS (2014) Endothelin-1 and its role in the pathogenesis of infectious diseases. Life Sci. E-pub ahead of print. doi:10.1016/j.lfs.2014.04.021

109. Machado FS, Desruisseaux MS, Nagajyothi, Kennan RP, Hetherington HP, et al. (2006) Endothelin in a murine model of cerebral malaria. Exp Biol Med (Maywood) 231: 1176–1181.

110. Dai M, Freeman B, Bruno FP, Shikani HJ, Tanowitz HB, et al. (2012) The novel ETA receptor antagonist HJP-272 prevents cerebral microvascular hemorrhage in cerebral malaria and synergistically improves survival in combination with an artemisinin derivative. Life Sci 91: 687–692.

111. Basilico N, Speciale L, Parapini S, Ferrante P, Taramelli D (2002) Endothelin-1 production by a microvascular endothelial cell line treated with Plasmodium falciparum parasitized red blood cells. Clin Sci (Lond) 103 Suppl 48: 464S–466S.

112. Wenisch C, Wenisch H, Wilairatana P, Looareesuwan S, Vannaphan S, et al. (1996) Big endothelin in patients with complicated Plasmodium falciparum malaria. J Infect Dis 173: 1281–1284.

113. Martins C, Tanowitz H, Weiss L, Desruisseaux MS (2014) Endothelin-1 treatment induces experimental cerebral malaria in *Plasmodium berghei* NK65 infected mice. Malaria 2014: Advances in Pathophysiology, Biology and Drug Development New York, NY: New York Academy of Sciences.

114. Sirvio ML, Metsarinne K, Saijonmaa O, Fyhrquist F (1990) Tissue distribution and half-life of 125I-endothelin in the rat: importance of pulmonary clearance. Biochem Biophys Res Commun 167: 1191–1195.

115. Willenborg DO, Staykova M, Fordham S, O'Brien N, Linares D (2007) The contribution of nitric oxide and interferon gamma to the regulation of the neuro-inflammation in experimental autoimmune encephalomyelitis. J Neuroimmunol 191: 16–25.

116. Ong PK, Melchior B, Martins YC, Hofer A, Orjuela-Sanchez P, et al. (2013) Nitric oxide synthase dysfunction contributes to impaired cerebroarteriolar reactivity in experimental cerebral malaria. PLoS Pathog 9: e1003444.

117. Orjuela-Sanchez P, Ong PK, Zanini GM, Melchior B, Martins YC, et al. (2013) Transdermal glyceryl trinitrate as an effective adjunctive treatment with artemether for late-stage experimental cerebral malaria. Antimicrob Agents Chemother 57: 5462–5471.

118. Zanini GM, Martins YC, Cabrales P, Frangos JA, Carvalho LJ (2012) S-nitrosoglutathione prevents experimental cerebral malaria. J Neuroimmune Pharmacol 7: 477–487.

119. Cabrales P, Zanini GM, Meays D, Frangos JA, Carvalho LJ (2011) Nitric oxide protection against murine cerebral malaria is associated with improved cerebral microcirculatory physiology. J Infect Dis 203: 1454–1463.

120. Serghides L, Kim H, Lu Z, Kain DC, Miller C, et al. (2011) Inhaled nitric oxide reduces endothelial activation and parasite accumulation in the brain, and enhances survival in experimental cerebral malaria. PLoS One 6: e27714.

121. Hawkes M, Opoka RO, Namasopo S, Miller C, Conroy AL, et al. (2011) Nitric oxide for the adjunctive treatment of severe malaria: hypothesis and rationale. Med Hypotheses 77: 437–444.

122. Imai T, Shen J, Chou B, Duan X, Tu L, et al. (2010) Involvement of CD8+ T cells in protective immunity against murine blood-stage infection with Plasmodium yoelii 17XL strain. Eur J Immunol 40: 1053–1061.

123. Voza T, Vigario AM, Belnoue E, Gruner AC, Deschemin J-C, et al. (2005) Species-specific inhibition of cerebral malaria in mice coinfected with Plasmodium spp. Infect Immun 73: 4777–4786.

124. Clark CJ, Phillips RS (2011) Cerebral malaria protection in mice by species-specific Plasmodium coinfection is associated with reduced CC chemokine levels in the brain. Parasite Immunol 33: 637–641.

125. Shivtiel S, Kollet O, Lapid K, Schajnovitz A, Goichberg P, et al. (2008) CD45 regulates retention, motility, and numbers of hematopoietic progenitors, and affects osteoclast remodeling of metaphyseal trabecules. J Exp Med 205: 2381–2395.

126. Silverberg J, Ginsburg D, Orman R, Amassian V, Durkin HG, et al. (2010) Lymphocyte infiltration of neocortex and hippocampus after a single brief seizure in mice. Brain Behav Immun 24: 263–272.

127. Cambiaggi C, Scupoli MT, Cestari T, Gerosa F, Carra G, et al. (1992) Constitutive expression of CD69 in interspecies T-cell hybrids and locus assignment to human chromosome 12. Immunogenetics 36: 117–120.

128. Tough DF, Sun S, Zhang X, Sprent J (1999) Stimulation of naive and memory T cells by cytokines. Immunol Rev 170: 39–47.

129. Fauconnier M, Palomo J, Bourigault ML, Meme S, Szeremeta F, et al. (2012) IL-12Rbeta2 is essential for the development of experimental cerebral malaria. J Immunol 188: 1905–1914.

130. Boubou MI, Collette A, Voegtle D, Mazier D, Cazenave PA, et al. (1999) T cell response in malaria pathogenesis: selective increase in T cells carrying the TCR V(beta)8 during experimental cerebral malaria. Int Immunol 11: 1553–1562.

131. Silva-Filho JL, Souza MC, Ferreira-Dasilva CT, Silva LS, Costa MF, et al. (2013) Angiotensin II is a new component involved in splenic T lymphocyte responses during Plasmodium berghei ANKA infection. PLoS One 8: e62999.

132. Boeuf PS, Loizon S, Awandare GA, Tetteh JK, Addae MM, et al. (2012) Insights into deregulated TNF and IL-10 production in malaria: implications for understanding severe malarial anaemia. Malar J 11: 253.

133. Anada Y, Igarashi Y, Kihara A (2007) The immunomodulator FTY720 is phosphorylated and released from platelets. Eur J Pharmacol 568: 106–111.

134. Kihara A, Igarashi Y (2008) Production and release of sphingosine 1-phosphate and the phosphorylated form of the immunomodulator FTY720. Biochim Biophys Acta 1781: 496–502.

135. Garcia JG, Liu F, Verin AD, Birukova A, Dechert MA, et al. (2001) Sphingosine 1-phosphate promotes endothelial cell barrier integrity by Edg-dependent cytoskeletal rearrangement. J Clin Invest 108: 689–701.

136. Schaphorst KL, Chiang E, Jacobs KN, Zaiman A, Natarajan V, et al. (2003) Role of sphingosine-1 phosphate in the enhancement of endothelial barrier integrity by platelet-released products. Am J Physiol Lung Cell Mol Physiol 285: L258–267.

137. Conroy AL, Glover SJ, Hawkes M, Erdman LK, Seydel KB, et al. (2012) Angiopoietin-2 levels are associated with retinopathy and predict mortality in Malawian children with cerebral malaria: a retrospective case-control study. Crit Care Med 40: 952–959.

138. Conroy AL, Lafferty EI, Lovegrove FE, Krudsood S, Tangpukdee N, et al. (2009) Whole blood angiopoietin-1 and -2 levels discriminate cerebral and severe (non-cerebral) malaria from uncomplicated malaria. Malar J 8: 295.

139. Lovegrove FE, Tangpukdee N, Opoka RO, Lafferty EI, Rajwans N, et al. (2009) Serum angiopoietin-1 and -2 levels discriminate cerebral malaria from uncomplicated malaria and predict clinical outcome in African children. PLoS ONE 4: e4912.

140. Jain V, Lucchi NW, Wilson NO, Blackstock AJ, Nagpal AC, et al. (2011) Plasma levels of angiopoietin-1 and -2 predict cerebral malaria outcome in Central India. Malar J 10: 383.

141. Senaldi G, Vesin C, Chang R, Grau GE, Piguet PF (1994) Role of polymorphonuclear neutrophil leukocytes and their integrin CD11a (LFA-1) in the pathogenesis of severe murine malaria. Infect Immun 62: 1144–1149.

142. Rossi B, Angiari S, Zenaro E, Budui SL, Constantin G (2011) Vascular inflammation in central nervous system diseases: adhesion receptors controlling leukocyte-endothelial interactions. J Leukoc Biol 89: 539–556.

143. Hunt NH, Golenser J, Chan-Ling T, Parekh S, Rae C, et al. (2006) Immunopathogenesis of cerebral malaria. Int J Parasitol 36: 569–582.

144. Medana IM, Hunt NH, Chan-Ling T (1997) Early activation of microglia in the pathogenesis of fatal murine cerebral malaria. Glia 19: 91–103.

145. Belnoue E, Kayibanda M, Deschemin JC, Viguier M, Mack M, et al. (2003) CCR5 deficiency decreases susceptibility to experimental cerebral malaria. Blood 101: 4253–4259.

146. Penet MF, Kober F, Confort-Gouny S, Le Fur Y, Dalmasso C, et al. (2007) Magnetic resonance spectroscopy reveals an impaired brain metabolic profile in mice resistant to cerebral malaria infected with Plasmodium berghei ANKA. J Biol Chem 282: 14505–14514.

147. Galea I, Felton LM, Waters S, van Rooijen N, Perry VH, et al. (2008) Immune-to-brain signalling: the role of cerebral CD163-positive macrophages. Neurosci Lett 448: 41–46.

148. Galea I, Palin K, Newman TA, Van Rooijen N, Perry VH, et al. (2005) Mannose receptor expression specifically reveals perivascular macrophages in normal, injured, and diseased mouse brain. Glia 49: 375–384.

149. Polfliet MM, Zwijnenburg PJ, van Furth AM, van der Poll T, Dopp EA, et al. (2001) Meningeal and perivascular macrophages of the central nervous system play a protective role during bacterial meningitis. J Immunol 167: 4644–4650.

150. Howland SW, Poh CM, Gun SY, Claser C, Malleret B, et al. (2013) Brain microvessel cross-presentation is a hallmark of experimental cerebral malaria. EMBO Mol Med 5: 916–931.

151. Wang NK, Lai CC, Liu CH, Yeh LK, Chou CL, et al. (2013) Origin of fundus hyperautofluorescent spots and their role in retinal degeneration in a mouse model of Goldmann-Favre syndrome. Dis Model Mech 6: 1113–1122.

152. Pai S, Qin J, Cavanagh L, Mitchell A, El-Assaad F, et al. (2014) Real-time imaging reveals the dynamics of leukocyte behaviour during experimental cerebral malaria pathogenesis. PLoS Pathog 10: e1004236.

153. Fernandez-Reyes D, Craig AG, Kyes SA, Peshu N, Snow RW, et al. (1997) A high frequency African coding polymorphism in the N-terminal domain of ICAM-1 predisposing to cerebral malaria in Kenya. Hum Mol Genet 6: 1357–1360.

154. Ockenhouse CF, Tegoshi T, Maeno Y, Benjamin C, Ho M, et al. (1992) Human vascular endothelial cell adhesion receptors for Plasmodium falciparum-infected erythrocytes: roles for endothelial leukocyte adhesion molecule 1 and vascular cell adhesion molecule 1. J Exp Med 176: 1183–1189.

155. Ochola LB, Siddondo BR, Ocholla H, Nkya S, Kimani EN, et al. (2011) Specific receptor usage in Plasmodium falciparum cytoadherence is associated with disease outcome. PLoS ONE 6: e14741.

156. Craig A, Fernandez-Reyes D, Mesri M, McDowall A, Altieri DC, et al. (2000) A functional analysis of a natural variant of intercellular adhesion molecule-1 (ICAM-1Kilifi). Hum Mol Genet 9: 525–530.

157. Silamut K, Phu NH, Whitty C, Turner GD, Louwrier K, et al. (1999) A quantitative analysis of the microvascular sequestration of malaria parasites in the human brain. Am J Pathol 155: 395–410.

158. Newbold C, Warn P, Black G, Berendt A, Craig A, et al. (1997) Receptor-specific adhesion and clinical disease in Plasmodium falciparum. Am J Trop Med Hyg 57: 389–398.

159. Pino P, Taoufiq Z, Nitcheu J, Vouldoukis I, Mazier D (2005) Blood-brain barrier breakdown during cerebral malaria: suicide or murder? Thromb Haemost 94: 336–340.

160. Grau GE, Tacchini-Cottier F, Vesin C, Milon G, Lou JN, et al. (1993) TNF-induced microvascular pathology: active role for platelets and importance of the LFA-1/ICAM-1 interaction. Eur Cytokine Netw 4: 415–419.

161. Favre N, Da Laperousaz C, Ryffel B, Weiss NA, Imhof BA, et al. (1999) Role of ICAM-1 (CD54) in the development of murine cerebral malaria. Microbes Infect 1: 961–968.

162. Li J, Chang WL, Sun G, Chen HL, Specian RD, et al. (2003) Intercellular adhesion molecule 1 is important for the development of severe experimental malaria but is not required for leukocyte adhesion in the brain. J Investig Med 51: 128–140.

163. Bauer PR, Van Der Heyde HC, Sun G, Specian RD, Granger DN (2002) Regulation of endothelial cell adhesion molecule expression in an experimental model of cerebral malaria. Microcirculation 9: 463–470.

164. Weiser S, Miu J, Ball HJ, Hunt NH (2007) Interferon-gamma synergises with tumour necrosis factor and lymphotoxin-alpha to enhance the mRNA and protein expression of adhesion molecules in mouse brain endothelial cells. Cytokine 37: 84–91.

165. Zhou H, Andonegui G, Wong CH, Kubes P (2009) Role of endothelial TLR4 for neutrophil recruitment into central nervous system microvessels in systemic inflammation. J Immunol 183: 5244–5250.

166. Zhou H, Lapointe BM, Clark SR, Zbytnuik L, Kubes P (2006) A requirement for microglial TLR4 in leukocyte recruitment into brain in response to lipopolysaccharide. J Immunol 177: 8103–8110.

167. Griffiths M, Neal JW, Gasque P (2007) Innate immunity and protective neuroinflammation: new emphasis on the role of neuroimmune regulatory proteins. Int Rev Neurobiol 82: 29–55.

168. Lloyd KL, Kubes P (2006) GPI-linked endothelial CD14 contributes to the detection of LPS. Am J Physiol Heart Circ Physiol 291: H473–481.

169. Oakley MS, Majam V, Mahajan B, Gerald N, Anantharaman V, et al. (2009) Pathogenic roles of CD14, galectin-3, and OX40 during experimental cerebral malaria in mice. PLoS ONE 4: e6793.

170. Devitt A, Moffatt OD, Raykundalia C, Capra JD, Simmons DL, et al. (1998) Human CD14 mediates recognition and phagocytosis of apoptotic cells. Nature 392: 505–509.

171. Wiese L, Hempel C, Penkowa M, Kirkby N, Kurtzhals JA (2008) Recombinant human erythropoietin increases survival and reduces neuronal apoptosis in a murine model of cerebral malaria. Malar J 7: 3.

172. Wiese L, Kurtzhals JA, Penkowa M (2006) Neuronal apoptosis, metallothionein expression and proinflammatory responses during cerebral malaria in mice. Exp Neurol 200: 216–226.

173. Lackner P, Burger C, Pfaller K, Heussler V, Helbok R, et al. (2007) Apoptosis in experimental cerebral malaria: spatial profile of cleaved caspase-3 and ultrastructural alterations in different disease stages. Neuropathol Appl Neurobiol 33: 560–571.

174. Ling ZL, Combes V, Grau GE, King NJ (2011) Microparticles as immune regulators in infectious disease - an opinion. Front Immunol 2: 67.

175. El-Assaad F, Wheway J, Hunt NH, Grau GE, Combes V (2014) Production, fate and pathogenicity of plasma microparticles in murine cerebral malaria. PLoS Pathog 10: e1003839.

176. Vasina EM, Cauwenberghs S, Feijge MA, Heemskerk JW, Weber C, et al. (2011) Microparticles from apoptotic platelets promote resident macrophage differentiation. Cell Death Dis 2: e211.

177. MacPherson GG, Warrell MJ, White NJ, Looareesuwan S, Warrell DA (1985) Human cerebral malaria a quantitative ultrastructural analysis of parasitized erythrocyte sequestration. ajp 119: 385–401.

178. Clark IA, Budd AC, Alleva LM, Cowden WB (2006) Human malarial disease: a consequence of inflammatory cytokine release. Malar J 5: 85.

179. Clark IA, Schofield L (2000) Pathogenesis of malaria. Parasitol Today 16: 451–454.

180. Grau GE, Pointaire P, Piguet PF, Vesin C, Rosen H, et al. (1991) Late administration of monoclonal antibody to leukocyte function-antigen 1 abrogates incipient murine cerebral malaria. Eur J Immunol 21: 2265–2267.

181. Falanga PB, Butcher EC (1991) Late treatment with anti-LFA-1 (CD11a) antibody prevents cerebral malaria in a mouse model. Eur J Immunol 21: 2259–2263.

182. Frevert U, Nacer A, Cabrera M, Movila A, Leberl M (2014) Imaging Plasmodium immunobiology in the liver, brain, and lung. Parasitol Int 63: 171–186.

183. van der Heyde HC, Gramaglia I, Sun G, Woods C (2005) Platelet depletion by anti-CD41 (alphaIIb) mAb injection early but not late in the course of disease protects against *Plasmodium berghei* pathogenesis by altering the levels of pathogenic cytokines. Blood 105: 1956–1963.

184. Sun G, Chang WL, Li J, Berney SM, Kimpel D, et al. (2003) Inhibition of platelet adherence to brain microvasculature protects against severe *Plasmodium berghei* malaria. Infect Immun 71: 6553–6561.

185. Granger DN, Senchenkova E (2010) Endothelial Barrier Dysfunction. Inflammation and the Microcirculation. San Rafael (CA): Morgan& Claypool Lifesciences.

186. Lawson C, Wolf S (2009) ICAM-1 signaling in endothelial cells. Pharmacol Rep 61: 22–32.

187. Sumagin R, Lomakina E, Sarelius IH (2008) Leukocyte-endothelial cell interactions are linked to vascular permeability via ICAM-1-mediated signaling. Am J Physiol Heart Circ Physiol 295: H969–H977.

188. Li N (2008) Platelet-lymphocyte cross-talk. J Leukoc Biol 83: 1069–1078.

189. Idro R, Carter JA, Fegan G, Neville BG, Newton CR (2006) Risk factors for persisting neurological and cognitive impairments following cerebral malaria. Arch Dis Child 91: 142–148.

190. van Hensbroek MB, Palmer A, Jaffar S, Schneider G, Kwiatkowski D (1997) Residual neurologic sequelae after childhood cerebral malaria. J Pediatr 131: 125–129.

191. Beare NA, Glover SJ, Lewallen S, Taylor TE, Harding SP, et al. (2012) Prevalence of raised intracranial pressure in cerebral malaria detected by optic nerve sheath ultrasound. Am J Trop Med Hyg 87: 985–988.

192. Idro R, Kakooza-Mwesige A, Balyejjussa S, Mirembe G, Mugasha C, et al. (2010) Severe neurological sequelae and behaviour problems after cerebral malaria in Ugandan children. BMC Res Notes 3: 104.

193. Frevert U, Nacer A (2014) Fatal cerebral malaria: a venous efflux problem. Front Cell Infect Microbiol 4: 155.

194. Idro R, Marsh K, John CC, Newton CR (2010) Cerebral malaria: mechanisms of brain injury and strategies for improved neurocognitive outcome. Pediatr Res 68: 267–274.

195. Zhao H, Aoshi T, Kawai S, Mori Y, Konishi A, et al. (2014) Olfactory plays a key role in spatiotemporal pathogenesis of cerebral malaria. Cell Host Microbe 15: 551–563.

196. Schmutzhard J, Kositz CH, Lackner P, Pritz C, Glueckert R, et al. (2011) Murine cerebral malaria: histopathology and ICAM 1 immunohistochemistry of the inner ear. Trop Med Int Health 16: 914–922.

197. Schmutzhard J, Kositz CH, Lackner P, Dietmann A, Fischer M, et al. (2010) Murine malaria is associated with significant hearing impairment. Malar J 9: 159.

198. Zhao SZ, Mackenzie IJ (2011) Deafness: malaria as a forgotten cause. Ann Trop Paediatr 31: 1–10.

199. Saggu R, Faille D, Grau GE, Cozzone PJ, Viola A (2011) In the Eye of Experimental Cerebral Malaria. Am J Pathol 179: 1104–1109.

200. Brewster DR, Kwiatkowski D, White NJ (1990) Neurological sequelae of cerebral malaria in children. Lancet 336: 1039–1043.

201. Dorovini-Zis K, Schmidt K, Huynh H, Fu W, Whitten RO, et al. (2011) The neuropathology of fatal cerebral malaria in malawian children. Am J Pathol 178: 2146–2158.

202. Milner DA, Jr., Valim C, Carr RA, Chandak PB, Fosiko NG, et al. (2013) A histological method for quantifying Plasmodium falciparum in the brain in fatal paediatric cerebral malaria. Malar J 12: 191.

203. White NJ, Turner GD, Day NP, Dondorp AM (2013) Lethal malaria: Marchiafava and Bignami were right. J Infect Dis 208: 192–198.

204. WHO (2011) World Malaria Report: 2011. Geneva, Switzerland: World Health Organization.

205. Mohan A, Sharma SK, Bollineni S (2008) Acute lung injury and acute respiratory distress syndrome in malaria. J Vector Borne Dis 45: 179–193.

206. Anstey NM, Jacups SP, Cain T, Pearson T, Ziesing PJ, et al. (2002) Pulmonary manifestations of uncomplicated *falciparum* and *vivax* malaria: cough, small airways obstruction, impaired gas transfer, and increased pulmonary phagocytic activity. J Infect Dis 185: 1326–1334.

207. Maguire GP, Handojo T, Pain MC, Kenangalem E, Price RN, et al. (2005) Lung injury in uncomplicated and severe *falciparum* malaria: a longitudinal study in papua, Indonesia. J Infect Dis 192: 1966–1974.

208. Sarkar D, Ray S, Saha M, Chakraborty A, Talukdar A (2013) Clinico-laboratory profile of severe Plasmodium vivax malaria in a tertiary care centre in Kolkata. Trop Parasitol 3: 53–57.

209. Sarkar S, Bhattacharya P (2008) Cerebral malaria caused by *Plasmodium vivax* in adult subjects. Indian J Crit Care Med 12: 204–205.

210. Bhattacharjee P, Dubey S, Gupta VK, Agarwal P, Mahato MP (2013) The clinicopathologic manifestations of *Plasmodium vivax* malaria in children: a growing menace. J Clin Diagn Res 7: 861–867.

211. Abdallah TM, Abdeen MT, Ahmed IS, Hamdan HZ, Magzoub M, et al. (2013) Severe *Plasmodium falciparum* and *Plasmodium vivax* malaria among adults at Kassala Hospital, eastern Sudan. Malar J 12: 148.

212. Gehlawat VK, Arya V, Kaushik JS, Gathwala G (2013) Clinical spectrum and treatment outcome of severe malaria caused by Plasmodium vivax in 18 children from northern India. Pathog Glob Health 107: 210–214.

213. Pinzon MA, Pineda JC, Rosso F, Shinchi M, Bonilla-Abadia F (2013) *Plasmodium vivax* cerebral malaria complicated with venous sinus thrombosis in Colombia. Asian Pac J Trop Med 6: 413–415.

214. Beg MA, Khan R, Baig SM, Gulzar Z, Hussain R, et al. (2002) Cerebral involvement in benign tertian malaria. Am J Trop Med Hyg 67: 230–232.

215. Thapa R, Patra V, Kundu R (2007) *Plasmodium vivax* cerebral malaria. Indian Pediatr 44: 433–434.

216. Andrade BB, Reis-Filho A, Souza-Neto SM, Clarencio J, Camargo LM, et al. (2010) Severe *Plasmodium vivax* malaria exhibits marked inflammatory imbalance. Malar J 9: 13.

217. Cromer D, Evans KJ, Schofield L, Davenport MP (2006) Preferential invasion of reticulocytes during late-stage *Plasmodium berghei* infection accounts for reduced circulating reticulocyte levels. Int J Parasitol 36: 1389–1397.

218. McNally J, O'Donovan SM, Dalton JP (1992) *Plasmodium berghei* and *Plasmodium chabaudi chabaudi*: development of simple *in vitro* erythrocyte invasion assays. Parasitology 105 (Pt 3): 355–362.

219. Russell B, Suwanarusk R, Borlon C, Costa FT, Chu CS, et al. (2011) A reliable ex vivo invasion assay of human reticulocytes by Plasmodium vivax. Blood 118: e74–81.

220. Panichakul T, Sattabongkot J, Chotivanich K, Sirichaisinthop J, Cui L, et al. (2007) Production of erythropoietic cells in vitro for continuous culture of *Plasmodium vivax*. Int J Parasitol 37: 1551–1557.

221. Vanderberg JP, Gwadz R (1980) The transmission by mosquitoes of *Plasmodia* in the laboratory. In: Kreier J, editor. Malaria: pathology, vector studies and culture. New York, N.Y.: Academic Press. pp. 154–218.

222. Franke-Fayard B, Trueman H, Ramesar J, Mendoza J, van der Keur M, et al. (2004) A *Plasmodium berghei* reference line that constitutively expresses GFP at a high level throughout the complete life cycle. Mol Biochem Parasitol 137: 23–33.

223. Yoeli M, Hargreaves BJ (1974) Brain capillary blockage produced by a virulent strain of rodent malaria. Science 184: 572–573.

224. Weiss L (1989) Mechanisms of splenic control of murine malaria: cellular reactions of the spleen in lethal (strain 17XL) *Plasmodium yoelii* malaria in BALB/c mice, and the consequences of pre-infective splenectomy. Am J Trop Med Hyg 41: 144–160.

225. Yoeli M, Hargreaves B, Carter R, Walliker D (1975) Sudden increase in virulence in a strain of *Plasmodium berghei yoelii*. Ann Trop Med Parasitol 69: 173–178.

226. Knop M, Barr F, Riedel CG, Heckel T, Reichel C (2002) Improved version of the red fluorescent protein (drFP583/DsRed/RFP). Biotechniques 33: 592–602.

227. Mikolajczak SA, Aly AS, Dumpit RF, Vaughan AM, Kappe SH (2008) An efficient strategy for gene targeting and phenotypic assessment in the *Plasmodium yoelii* rodent malaria model. Mol Biochem Parasitol 158: 213–216.

228. Tarun AS, Baer K, Dumpit RF, Gray S, Lejarcegui N, et al. (2006) Quantitative isolation and *in vivo* imaging of malaria parasite liver stages. Int J Parasitol 36: 1283–1293.

229. Nie CQ, Bernard NJ, Norman MU, Amante FH, Lundie RJ, et al. (2009) IP-10-mediated T cell homing promotes cerebral inflammation over splenic immunity to malaria infection. PLoS Pathog 5: e1000369.

230. Rest JR (1982) Cerebral malaria in inbred mice. I. A new model and its pathology. Trans Royal Soc Trop Med Hyg 76: 410–415.
231. Van den Steen PE, Deroost K, Van Aelst I, Geurts N, Martens E, et al. (2008) CXCR3 determines strain susceptibility to murine cerebral malaria by mediating T lymphocyte migration toward IFN-gamma-induced chemokines. Eur J Immunol 38: 1082–1095.
232. Amante FH, Stanley AC, Randall LM, Zhou Y, Haque A, et al. (2007) A role for natural regulatory T cells in the pathogenesis of experimental cerebral malaria. Am J Pathol 171: 548–559.
233. Grau GE, Heremans H, Piguet PF, Pointaire P, Lambert PH, et al. (1989) Monoclonal antibody against interferon gamma can prevent experimental cerebral malaria and its associated overproduction of tumor necrosis factor. Proc Natl Acad Sci USA 86: 5572–5574.
234. Grau GE, Piguet PF, Engers HD, Louis JA, Vassalli P, et al. (1986) L3T4+ T lymphocytes play a major role in the pathogenesis of murine cerebral malaria. J Immunol 137: 2348–2354.
235. Hearn J, Rayment N, Landon DN, Katz DR, de Souza JB (2000) Immunopathology of cerebral malaria: morphological evidence of parasite sequestration in murine brain microvasculature. Infect Immun 68: 5364–5376.
236. Jennings VM, Actor JK, Lal AA, Hunter RL (1997) Cytokine profile suggesting that murine cerebral malaria is an encephalitis. Infect Immun 65: 4883–4887.
237. Jennings VM, Lal AA, Hunter RL (1998) Evidence for multiple pathologic and protective mechanisms of murine cerebral malaria. Infect Immun 66: 5972–5979.
238. Kamiyama T, Tatsumi M, Matsubara J, Yamamoto K, Rubio Z, et al. (1987) Manifestation of cerebral malaria-like symptoms in the WM/Ms rat infected with Plasmodium berghei strain NK65. J Parasitol 73: 1138–1145.
239. Lacerda-Queiroz N, Rodrigues DH, Vilela MC, Miranda ASd, Amaral DCG, et al. (2010) Inflammatory changes in the central nervous system are associated with behavioral impairment in Plasmodium berghei (strain ANKA)-infected mice. Exp Parasitol 125: 271–278.
240. Mackey LJ, Hochmann A, June CH, Contreras CE, Lambert PH (1980) Immunopathological aspects of Plasmodium berghei infection in five strains of mice. II. Immunopathology of cerebral and other tissue lesions during the infection. Clin Exp Immunol 42: 412–420.
241. Patel SN, Berghout J, Lovegrove FE, Ayi K, Conroy A, et al. (2008) C5 deficiency and C5a or C5aR blockade protects against cerebral malaria. J Exp Med 205: 1133–1143.
242. Yanez DM, Manning DD, Cooley AJ, Weidanz WP, van der Heyde HC (1996) Participation of lymphocyte subpopulations in the pathogenesis of experimental murine cerebral malaria. J Immunol 157: 1620–1624.
243. Polder TW, Jerusalem CR, Eling WMC (1991) Morphological characteristics of intracerebral arterioles in clinical (Plasmodium falciparum) and experimental (Plasmodium berghei) cerebral malaria. J Neurol Sci 101: 35–46.
244. McElroy PD, Beier JC, Oster CN, Onyango FK, Oloo AJ, et al. (1997) Dose- and time-dependent relations between infective Anopheles inoculation and outcomes of Plasmodium falciparum parasitemia among children in western Kenya. Am J Epidemiol 145: 945–956.
245. Hatcher JP, Jones DN, Rogers DC, Hatcher PD, Reavill C, et al. (2001) Development of SHIRPA to characterise the phenotype of gene-targeted mice. Behav Brain Res 125: 43–47.
246. Carroll RW, Wainwright MS, Kim KY, Kidambi T, Gomez ND, et al. (2010) A rapid murine coma and behavior scale for quantitative assessment of murine cerebral malaria. PLoS ONE 5: pii: e13124.
247. Frevert U, Engelmann S, Zougbédé S, Stange J, Ng B, et al. (2005) Intravital observation of Plasmodium berghei sporozoite infection of the liver. PLoS Biol 3: e192.
248. Baer K, Klotz C, Kappe SH, Schnieder T, Frevert U (2007) Release of hepatic Plasmodium yoelii merozoites into the pulmonary microvasculature. PLoS Pathog 3: e171.
249. Becker MD, Nobiling R, Planck SR, Rosenbaum JT (2000) Digital video-imaging of leukocyte migration in the iris: intravital microscopy in a physiological model during the onset of endotoxin-induced uveitis. J Immunol Methods 240: 23–37.
250. Cabrera M, Pewe LL, Harty JT, Frevert U (2013) In vivo CD8+ T cell dynamics in the liver of Plasmodium yoelii immunized and infected mice. PLoS One 8: e70842.
251. Gundra UM, Mishra BB, Wong K, Teale JM (2011) Increased disease severity of parasite-infected TLR2-/- mice is correlated with decreased central nervous system inflammation and reduced numbers of cells with alternatively activated macrophage phenotypes in a murine model of neurocysticercosis. Infect Immun 79: 2586–2596.
252. Irani DN, Griffin DE (1991) Isolation of brain parenchymal lymphocytes for flow cytometric analysis. Application to acute viral encephalitis. J Immunol Methods 139: 223–231.
253. Mishra BB, Gundra UM, Wong K, Teale JM (2009) MyD88-deficient mice exhibit decreased parasite-induced immune responses but reduced disease severity in a murine model of neurocysticercosis. Infect Immun 77: 5369–5379.
254. Cabrera M, Frevert U (2012) Novel in vivo imaging techniques for the liver microvasculature. IntraVital 1: 107–114.